ELSEVIER

Dispersive and friction-induced stabilization of the Cahn–Hilliard inverse cascade

Bernard Legras [a,*], Barbara Villone [b]

[a] *Laboratoire de Météorologie Dynamique, Ecole Normale Superieure, UMR8539, 24 rue Lhomond, 75231 Paris Cedex 5, France*
[b] *Istituto di Fisica dello Spazio Interplanetariò, CNR, Corso Fiume 4, 10133 Turin, Italy*

Abstract

We discuss the stabilization of the inverse cascade in the large-scale instability of the Kolmogorov flow described by the complete Cahn–Hilliard equation with inclusion of β effect, large-scale friction and deformation radius. The friction and the β values halting the inverse cascade at the various possible intermediate states are calculated by means of singular perturbation techniques and compared to the values resulting from numerical simulation of the complete Cahn–Hilliard equation. The excellent agreement validates the theory. Our main result is that the critical values of friction or β halting the inverse cascade scale exponentially as a function of the jet separation in the final flow, contrary to previous theories and phenomenological approach.
© 2002 Elsevier Science B.V. All rights reserved.

1. Introduction

Inverse cascades are a common feature in the large-scale velocity and magnetic fields of geophysical, planetary and astrophysical two-dimensional flows. Their halting by spontaneous formation of zonal jets has been the object of great interest and considerable work by many scientists (see among others Refs. [1–5]). The phenomenon of a halted inverse cascade could play a role in the atmosphere of Jupiter and other Jovian planets which exhibit jet streams of east–west and west–east circulation.

Frisch et al. [6] showed that the inverse cascade of the large-scale nonlinear instability of the Kolmogorov flow described by the Cahn–Hilliard equation [7–9] may be stopped by the dispersive Rossby waves, i.e. by the so-called β-effect. We recall here that in the absence of any stabilizing effect the inverse cascade proceeds by visiting a family of metastable states with increasing scale until the final largest scale is reached [10]. In a later paper, Legras et al. [11] have used singular perturbation techniques to calculate the range of the β values stopping the inverse

---

* Corresponding author. Tel.: +33-1-44-32-22-28; fax: +33-1-43-36-83-92.
E-mail address: legras@lmd.ens.fr (B. Legras).

cascade in one of the otherwise (if $\beta = 0$) metastable state. Their result was different from that obtained by the standard phenomenology based on dimensional arguments [1] which fails because phenomenology does not take into account the strong suppression of nonlinearities in the metastable states of the inverse cascade.

In Refs. [6,11] the forcing maintaining the basic flow was chosen parallel to the planetary vorticity contours and there was no friction or advection. In a more realistic setup, Manfroi and Young [5] studied the stability of a forced meridional flow on a β-plane pushing the fluid across the planetary vorticity contours, and including both friction and advection by a mean flow. They obtained a complete amplitude equation for the leading order perturbation, from which, with some formal modifications and with a slightly different interpretation of the parameters, the amplitude equation of Ref. [6] can be recovered (see Section 2.1). Using this equation, but disregarding the dispersive contribution from β-effect, they showed that random initial perturbations rapidly reorganize into a set of fast and narrow eastward jets separated by slower and broader westward jets, followed then by a much slower adjustment of the jets, involving gradual migration and merger. The stabilization discussed in Ref. [5] is only due to friction and not due to dispersive effects.

In this paper we present a systematic approach to the study of stabilization of the inverse cascade in the supercritical regime of the large-scale Kolmogorov flow provided both by friction and β effect. The stabilization by β effect already discussed in [11] will be presented here in a greater detail and stabilization by friction will be discussed in the same mathematical approach as for the β case. The mathematical framework is based on the kink dynamics introduced by Kawasaki and Ohta [12] to describe the solutions to the Cahn–Hilliard equation; singular perturbation technique is used to study the stability of these solutions with respect to small perturbations due to friction and β effect. The perturbative calculations are performed analytically for large wavenumbers and numerically for all cases. The results are compared together and with direct numerical stability and time-dependent solutions of the amplitude equation.

The paper is organized as follows: in Section 2 the Cahn–Hilliard equation in its *complete* form is presented; by *complete* in this context we mean that β, friction, advection velocity and deformation terms have been added to the standard Cahn–Hilliard equation. The perturbation to the steady metastable solution of the Cahn–Hilliard equation by small β and a friction term is presented in Section 3. Section 4 discusses the stability of the steady metastable solutions and provides the main results of this work. Section 5 presents the techniques used to solve numerically the perturbation and the time-dependent problem, and compares the results of those calculations and the analytical results. Section 6 offers a summary and conclusions.

We do not give the detailed presentation of the mean advection effect, which introduces considerable additional algebraic complications, in order to focus here on the essential mechanisms that stabilizes the Cahn–Hilliard cascade. The main results in presence of mean advection are, however, given without demonstration in Appendix D.

2. The complete Cahn–Hilliard equation

2.1. Basic equation

Our starting point is the large-scale Kolmogorov flow in its slightly supercritical regime, which is described by the Cahn–Hilliard equation. We recall here that the basic Kolmogorov flow, $\mathbf{u} = (\cos y, 0)$, is maintained by a force $\mathbf{f} = \nu(\cos y, 0)$ against viscous dissipation. This flow exhibits a large-scale instability of the negative eddy viscosity type when the kinematic viscosity ν is slightly below the critical value $\nu_c = 1/\sqrt{2}$ [7–9].

Taking further into account β effect, friction r, external deformation radius $1/S$[1] and advection effect due to a nonzero mean velocity γ, we obtain by multi-scale techniques the following adimensional equation for the leading

---

[1] The external deformation radius accounts for the inertial large-scale effect of a free surface in geophysical flows [13].

order large-scale perturbation:

$$\partial_t (1 - S^2 \partial_x^{-2})(v - \gamma) = \lambda \partial_x^2 W'(v) - \lambda \partial_x^4 v - \beta \partial_x^{-1}(v - \gamma) - r(v - \gamma), \tag{1}$$

where ∂_x^{-1} denotes the integration in x defined for the family of functions with zero average over the interval $[0, L]$. The potential $W(v)$ is

$$W(v) = \frac{s^2}{2\Gamma^2} v^4 - s^2 v^2 \tag{2}$$

and the constants in (1) and (2) are

$$s = \frac{1}{\sqrt{3}}, \qquad \Gamma = \sqrt{\frac{3}{2}}, \qquad \lambda = \frac{3}{\sqrt{2}}. \tag{3}$$

Eq. (1) was derived in [6] with $S = r = \gamma = 0$. In this derivation, the Kolmogorov basic flow is oriented in the zonal direction on the β-plane and therefore the large amplitude flow develops in the meridional direction. Using a more realistic setting where the Kolmogorov basic flow is oriented in the meridional direction as an idealized baroclinic perturbation, and introducing friction and mean advection velocity, Manfroi and Young [5] derived the following amplitude equation:

$$\partial_\tau A = -r^* A - (2 - \gamma^{*2}) \partial_\eta^2 A - 3\partial_\eta^4 A + 2\gamma^* \partial_\eta (\partial_\eta A)^2 + \tfrac{2}{3} \partial_\eta (\partial_\eta A)^3 - \beta^* \partial_\eta^{-1} A, \tag{4}$$

where τ and η are the temporal and spatial variables, respectively. In their study, the last term on the right-hand side, which is the only dispersive term in the equation, was set to zero.[2] By the change of variable $\partial_\eta A = w - \gamma^*$ and the rescaling $\tau = at$, $\eta = bx$, $w = cv$, $r^* = r/a$, $\beta^* = \beta/(ab)$ and $\gamma^* = c\gamma$ where $a = 12s^4\lambda/(2 + \gamma^{*2})^2$, $b = (6s^2/(2 + \gamma^{*2}))^{1/2}$ and $c = (3(2 + \gamma^{*2})/(2\Gamma^2))^{1/2}$, this equation is easily transformed into (1) up to the term in S which is only a trivial modification [13]. We see that the quadratic term in (4) disappears in this transformation. The γ term represents the net advection velocity (see [5]) and is also the average value of v.

In a recent work [14], it is claimed that the Kolmogorov instability exhibits a singular limit when $\beta \to 0$. This result is established for a very special situation which does not arise here [15]. A more general approach for the stability of Rossby waves is given by Lee and Smith [16].

2.2. Kinks and antikinks

The pure Cahn–Hilliard equation, is recovered from (1) by setting $\beta = r = S = \gamma = 0$. It admits a variational formulation in terms of a Lyapunov functional [8]:

$$\partial_t \psi(x, t) = -\frac{\delta F}{\delta \psi},$$

where $\psi = \partial_x^{-1} v$ and F the Lyapunov functional with

$$\int_0^L \left(\frac{\lambda}{2} (\partial_x v)^2 + \lambda W(v) \right) \, \mathrm{d}x.$$

Consequently, the pure Cahn–Hilliard equation is integrable and all solutions tend to final steady states that locally minimize F.

---

[2] The coefficient β in the last term of the right-hand side of (4) is the product of the planetary vorticity gradient per the small angle between the Kolmogorov flow direction and the planetary vorticity gradient. Therefore it can be either positive or negative unlike in the derivation of Ref. [6] where it is always positive.
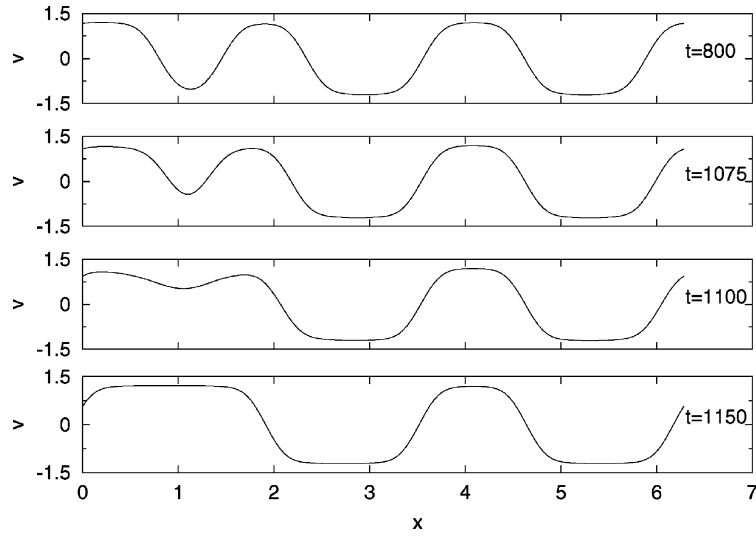
Fig. 1. Kink–antikink annihilation in a numerical simulation of the pure Cahn–Hilliard equation with $L = 76.95$.

This property is preserved in the presence of friction (see Section 5.5) but is lost in the presence of β.[3] The solutions to the pure Cahn–Hilliard equation live essentially, albeit some initial transients, within a slow manifold of soliton-like solutions with an alternation of plateaus $v = \pm\Gamma$, separated by alternating positive and negative kinks, that we will call, respectively, kinks and antikinks [17] in the following. For large enough separation between adjacent kinks, the kink centered in $x = x_j$ is locally given by

$$M_j(x) = \epsilon_j M(x - x_j) = \epsilon_j \Gamma \tanh s(x - x_j), \tag{5}$$

where $\epsilon_j = 1$ for a kink and $\epsilon_j = -1$ for an antikink [12]. This solution satisfies the equation

$$-\partial_x^2 M_j + W'(M_j) = 0.$$

Within an x periodic domain of period L, the Cahn–Hilliard equation exhibits stationary metastable solutions of period $\Lambda = L/N$ with N pairs of alternating and equally spaced kinks and antikinks. These fixed points are unstable saddle points of the Lyapunov functional, except for $N = 1$ which corresponds to an absolute stable minimum. The temporal evolution characterized by a growing total energy is a cascade of annihilations of kink–antikink pairs (see Fig. 1) leading eventually to the gravest mode $N = 1$ [12]. It is shown in Appendix A that the local solution (5) is modified by terms of order $\exp(-s\Lambda)$ when the periodicity is taken into account.

3. Perturbation of stationary solution under the action of β and friction

In order to study the modification of the stationary solutions to the pure Cahn–Hilliard equation under the effect of a small β or friction, we multiply both terms by a small control parameter, ε, keeping β and r as O(1).

We put $\gamma = 0$, leaving the case $\gamma \neq 0$, which is technically much more involved, for Appendix D. We only notice here that $\gamma \neq 0$ breaks one symmetry and generates narrow intense westerlies and broad narrow easterlies [5].

---

[3] A Lyapunov formulation for the approximated equation is recovered, however, in the limit of large β [6].

It is convenient to integrate (1) twice in x to obtain

$$-\frac{1}{\lambda}\partial_x^{-2}(1-S^2\partial_x^{-2})\partial_t v - \varepsilon\frac{\beta}{\lambda}\partial_x^{-3}v - \varepsilon\frac{r}{\lambda}\partial_x^{-2}v = \partial_x^2 v - W'(v) + h(t),\tag{6}$$

where $h(t)$ arises from integration in x. Then the perturbed solution is defined as $\bar{v} = \bar{v}^{(0)} + \varepsilon\bar{v}^{(1)} + \varepsilon^2\bar{v}^{(2)} + \mathrm{O}(\varepsilon^3)$, where $\bar{v}^{(0)}$ satisfies the stationary CH equation $-\partial_x^2\bar{v}^{(0)} + U'(\bar{v}^{(0)}) = 0$. We will distinguish two cases for S: (i) $S = 0$, associated with synoptic and subsynoptic dynamics, and (ii) $S = \mathrm{O}(1)$, associated with planetary motion (cf. [13]). When $\beta \neq 0$, we introduce the phase velocity $c = \varepsilon c_1 + \varepsilon^2 c_2 + \mathrm{O}(\varepsilon^3)$ of the traveling framework in which $\bar{v}$ is stationary.

3.1. Order 1 perturbation

We first treat the case $S = 0$. The first-order perturbation $\bar{v}^{(1)}$ satisfies the linear equation

$$\mathcal{F}(\bar{v}^{(1)}) = Q^{(0)}\tag{7}$$

with

$$\mathcal{F}(g) = \partial_x^2 g - W_0'' g, \quad W_0'' = W''(\bar{v}^{(0)}), \qquad Q^{(0)} = \frac{1}{\lambda}(c_1\partial_x^{-1}\bar{v}^{(0)} - \beta\partial_x^{-3}\bar{v}^{(0)} - r\partial_x^{-2}\bar{v}^{(0)}).$$

$\partial_x\bar{v}^{(0)}$ belongs to the kernel of $\mathcal{F}$: this can be easily verified by multiplying (7) by $\partial_x\bar{v}^{(0)}$ and integrating within the domain. After integration over the spatial period, the solvability condition for (7) gives the first-order contribution to the phase velocity

$$c_1 = -\beta\frac{\int_0^L(\partial_x^{-1}\bar{v}^{(0)})^2\,\mathrm{d}x}{\int_0^L(\bar{v}^{(0)})^2\,\mathrm{d}x}.\tag{8}$$

The symmetry of the stationary Cahn–Hilliard equation with respect to x reversal is inherited by $\bar{v}^{(0)}$. The solution is antisymmetric with respect to kinks locations and symmetric with respect to the middle of the plateaus. The perturbation $\bar{v}^{(1)}$ is the sum of two parts

$$\bar{v}^{(1)} = \beta\bar{v}_\beta^{(1)} + r\bar{v}_r^{(1)},$$

where $\bar{v}_r^{(1)}$ has the same symmetry as $\bar{v}^{(0)}$ and $\bar{v}_\beta^{(1)}$ has opposite symmetry.

It is shown in Appendix A that, up to errors of $\mathrm{O}(\mathrm{e}^{-s\Lambda/2})$ the basic solution $\bar{v}^{(0)}$ can be approximated by a series of jumps locally described by (5). Over each interval $[x_j - \Lambda/4, x_j + \Lambda/4]$ centered on a kink in x_j (see (5)), we have

$$\partial_x^{-1}\bar{v}^{(0)} = \epsilon_j\frac{\Gamma}{s}\ln\left(\frac{\cosh sx}{\cosh(1/4)s\Lambda}\right) + \mathrm{O}(\mathrm{e}^{-s\Lambda/2}),$$

from which the velocity c_1 is readily calculated using (8). After some algebra, we get

$$c_1 = -\beta\left(\frac{\Lambda^2}{48} - \frac{\pi^2}{12s^2} + \frac{13\zeta(3)}{8\Lambda s^3}\right)\left(1 - \frac{4}{\Lambda s}\right)^{-1} + \mathrm{O}(\mathrm{e}^{-s\Lambda/2}),\tag{9}$$

where ζ is the Riemann zeta function. The phase velocity is directed to the left when $\beta > 0$ and increases with the wavelength Λ. The fact that the error in (9) is exponentially small makes this expression very accurate even for not so large values of Λ as we shall check below. By straightforward algebra, one gets

$$Q^{(0)} = -\frac{\beta\Gamma}{2\lambda}|x|\left(\frac{x^2}{3} - \frac{1}{4}\Lambda|x| + \frac{1}{24}\Lambda^2\right) - \frac{r\Gamma}{2\lambda}|x|\left(|x| - \frac{1}{2}\Lambda\right) + \mathrm{O}(\beta\Lambda^2 + r\Lambda).\tag{10}$$

Far from the kinks the ratio between the derivative and the potential term in $\mathcal{F}$ is $O(1/\Lambda^2)$. At leading order in $1/\Lambda$:

$$\bar{v}_\beta^{(1)} = \frac{\Gamma}{24s^2\lambda}|x|\left(|x| - \frac{1}{2}\Lambda\right)\left(|x| - \frac{1}{4}\Lambda\right),\tag{11}$$

$$\bar{v}_r^{(1)} = \frac{\Gamma}{8s^2\lambda}x\left(|x| - \frac{1}{2}\Lambda\right).\tag{12}$$

These expressions are valid in the interval $[-\Lambda/2, \Lambda/2]$ far from the kinks. It can be shown that at $O(1)$ distance from the kinks, $\bar{v}_\beta^{(1)}$ is $O(\Lambda^2)$, while $\bar{v}_r^{(1)}$ is $O(\Lambda)$.

For $S = O(1)$, the leading contribution of friction is unchanged, but the effect of β is deeply affected. $Q^{(0)}$ is modified as

$$Q_S^{(0)} = \frac{1}{\lambda}(c_1\partial_x^{-1}\bar{v}^{(0)} - (\beta + c_1 S^2)\partial_x^{-3}\bar{v}^{(0)} - r\partial_x^{-2}\bar{v}^{(0)}).$$

Therefore, the phase speed is now

$$c_{1S} = -\frac{\beta c_1}{S^2 c_1 + \beta},$$

where c_1 is given by (9), i.e.:

$$c_{1S} = -\frac{\beta}{S^2} + \frac{48\beta}{\Lambda^2 S^4} + O\left(\frac{\beta}{\Lambda^3}\right).\tag{13}$$

Unlike the infinite radius case, the phase speed varies weakly with Λ. Reporting (13) in $Q_S^{(0)}$ and solving for $\bar{v}_\beta^{(1)}$, we obtain

$$\bar{v}_\beta^{(1)} = \frac{\Gamma}{s^2 S^2 \Lambda\lambda}|x|\left(|x| - \frac{1}{4}\Lambda\right)\left(1 - 2\frac{|x|}{\Lambda}\right) + O(1)\tag{14}$$

at large distance from the kinks. The correction to the stationary solution scales as Λ and is considerably reduced with respect to the case $S = 0$, for which it scales as Λ^3.

4. Stability

4.1. Stability of the Cahn–Hilliard equation

The stability of the solution $v = 0$ is easily obtained by linearizing (1) in the Fourier domain. When $r = 0$, the solution is unstable to all Fourier modes with wavenumber $0 < k < k_m = \sqrt{2}s = \sqrt{2/3}$. This result does not depend on the values of β and S. When $r > 0$ the modes near $k = 0$ and k_m are stabilized and the instability band in k-space shrinks as r grows. The solution $v = 0$ is stable for $r > r_0 = \lambda s^4 = (3\sqrt{2})^{-1}$. The vicinity of this value has been studied in [5]. We are here interested in the limit of small r.

The stability of the nonzero stationary solutions to the Cahn–Hilliard equation can be studied using the equation for kink motion derived in Appendix B. For an arbitrary perturbation, fast transients dissipate rapidly, leaving only after a short time the part of the perturbation that projects onto kink displacement. The jth kink being displaced by δx_j, the perturbation to $\bar{v}^{(0)}$ is

$$\delta v = -\sum_{\ell=0}^{2N-1} \partial_x M_\ell \delta x_\ell.\tag{15}$$

Then using (B.14), the equation for the displacements is

$$-\frac{4\Gamma^2}{\lambda}\sum_{\ell=0}^{2N-1}\left((-1)^{j-\ell}\mathcal{G}_2(x_j-x_\ell)+(-1)^{j-\ell}\frac{\pi^2}{12Ls^2}-\frac{1}{2s}\delta_{j-\ell}\right)\delta\dot{x}_\ell$$

$$=64s^3\Gamma^2\,\mathrm{e}^{-s\Lambda}[2\delta x_j-\delta x_{j+1}-\delta x_{j-1}]-2\Gamma\epsilon_j\delta h. \tag{16}$$

It is convenient to use Fourier components defined as

$$\delta x_j=\sum_{m=0}^{2N-1}\psi_m\,\mathrm{e}^{\mathrm{i}\pi(mj/N)}$$

with $m\in[0,2N-1]$ and $\psi_{2N-m}=\overline{\psi_m}$. The equation for ψ_m is obtained by multiplying (16) by $(1/2N)\,\mathrm{e}^{-\mathrm{i}\pi(mj/N)}$ and summing over the j from 0 to $2N-1$. Taking into account the regular alternation of kinks and antikinks separated by intervals of length $L/2N$ in the basic solution and using the Fourier transform of the Green function given by (C.2), one obtains after some algebra:

$$\frac{1}{\lambda}\left(\frac{\Lambda}{1+\cos\theta_m}-\frac{2}{s}\right)\dot{\psi}_m=128s^3\,\mathrm{e}^{-s\Lambda}(1-\cos\theta_m)\psi_m-4\frac{N}{\Gamma}\delta h\delta(N-m) \tag{17}$$

with $\theta_m=\pi m/N$. The leading order form of (17) was given by Kawasaki and Ohta [12] with a factor 2 error (see Appendix B).

The first term in the right-hand side of (17) is destabilizing the stationary solution with the eigenvalue

$$\sigma_0=\frac{128s^3\lambda\,\mathrm{e}^{-s\Lambda}}{\Lambda}\sin^2\theta_m\left(1-\frac{2(1+\cos\theta_m)}{s\Lambda}\right)^{-1}. \tag{18}$$

This instability is responsible of the inverse cascade in the CH equation. Each value of m is associated with a real eigenvalue of $\mathcal{F}$ and a dimension 2 eigenspace. It turns out that an appropriate basis of this eigenspace is provided by the couple of orthogonal vectors

$$v_a(x)=\sum_{j=0}^{2N-1}(-1)^j\cos j\theta_m\partial_x M(x-x_j), \tag{19}$$

$$v_b(x)=\sum_{j=0}^{2N-1}(-1)^j\sin j\theta_m\partial_x M(x-x_j), \tag{20}$$

which are here given up to an error $\mathrm{O}(\mathrm{e}^{-s\Lambda/2})$. These expressions agree very well with the numerical solution shown in Fig. 2.

The δh contribution vanishes but on the mode $m=N$. The solution $v(x,t)$ must average to zero within the periodic interval $[0,L]$. In terms of kink motion, this imposes the constraint

$$\sum_{\ell=0}^{2N-1}(-1)^\ell\delta\dot{x}_\ell=0$$

and thus, $\dot{\psi}_N=0$. The presence of $\delta h(t)$ in (17) is required to impose this condition.
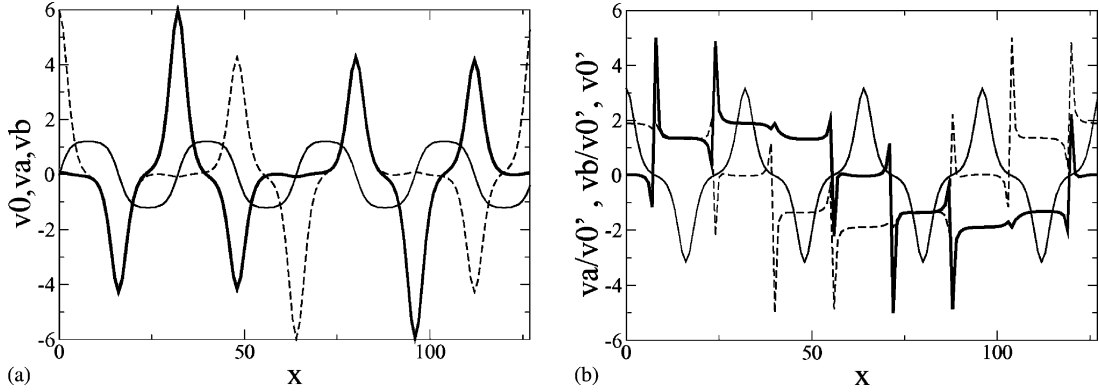
Fig. 2. Numerical calculation of v_a and v_b by discretization of the eigenvalue problem for $\mathcal{F}$ (cf. Section 5.1) with 128 points for $L = 76.953$ and $m = 4$. (a) Thin solid: $\bar{v}^{(0)}$, solid: v_a, dash: v_b; (b) thin solid: $\partial_x \bar{v}^{(0)}$, solid: $v_a/\partial_x \bar{v}^{(0)}$, dash: $v_b/\partial_x \bar{v}^{(0)}$. The scale is arbitrary for v_a and v_b. Even if the plateaus in $\bar{v}^{(0)}$ are very short for the chosen values of L and m, the ratios in (b) show the staircase structure of v_a and v_b over the kinks as given in (19) and (20) except where $\partial_x \bar{v}^{(0)}$ vanishes in the middle of the plateaus.

4.2. Stability of β-CH equation with infinite radius of deformation

4.2.1. Formulation of the problem

The equation governing the perturbation δv to $\bar{v}^{(0)}$ can be written conveniently for $\varphi = \partial_x^{-1} \delta v$

$$\partial_t \varphi = \mathcal{L}\varphi \tag{21}$$

with

$$\mathcal{L} = -\lambda \partial_x (\partial_x^2 - W''(\bar{v}))\partial_x - c\partial_x - \varepsilon\beta\partial_x^{-1} - \varepsilon r. \tag{22}$$

The reason of using φ instead of δv is that $\mathcal{L}$ is self-adjoint while the corresponding operator for δv is not.

Unlike the case $\beta = 0$, the slow component perturbation to the stationary solution of the β-CH equation does not reduce to the simple motion of kinks. One has also to take into account the dispersive effect of the β term modifying the shape of the slow modes and contributing to the stability. Therefore, we expand $\mathcal{L}$ as

$$\mathcal{L} = \mathcal{L}_0 + \varepsilon\mathcal{L}_1 + \varepsilon^2\mathcal{L}_2 + \mathrm{O}(\varepsilon^3) \tag{23}$$

with

$$\mathcal{L}_0 = -\lambda \partial_x (\partial_x^2 - U_0'')\partial_x, \tag{24}$$

$$\mathcal{L}_1 = \lambda \partial_x (W_0''' \bar{v}^{(1)} \partial_x) + c_1 \partial_x - \beta\partial_x^{-1} - r, \tag{25}$$

$$\mathcal{L}_2 = \lambda \partial_x (W_0''' \bar{v}^{(2)} + \tfrac{1}{2} W_0^{IV} \bar{v}^{(1)^2})\partial_x + c_2 \partial_x. \tag{26}$$

The eigenvalues of (21) are perturbations of the eigenvalues of (16). For a given $m \neq N$, we obtain

$$\sigma = \sigma_0 + \varepsilon\sigma_1 + \mathrm{i}\varepsilon\mu_1 + \varepsilon\sigma_2 + \mathrm{i}\varepsilon\mu_2 + \mathrm{O}(\varepsilon^3). \tag{27}$$

The functions $\varphi_a = \partial_x^{-1} v_a$ and $\varphi_b = \partial_x^{-1} v_b$ are orthogonal eigenmodes of $\mathcal{L}_0$ and, it turns out, an appropriate Jordan basis for the perturbation problem. They are, respectively, modified as $\varphi_a + \varepsilon\varphi_{a1} + \varepsilon^2\varphi_{a2} + \mathrm{O}(\varepsilon^3)$ and $\varphi_b + \varepsilon\varphi_{b1} + \varepsilon^2\varphi_{b2} + \mathrm{O}(\varepsilon^3)$. The hierarchy of linear problems is

$$\mathcal{L}_0\varphi_a = \sigma_0\varphi_a, \tag{28}$$

$$\mathcal{L}_0\varphi_{a1} + \mathcal{L}_1\varphi_a = \sigma_0\varphi_{a1} + \sigma_1\varphi_a - \mu_1\varphi_b, \tag{29}$$

$$\mathcal{L}_0\varphi_{a2} + \mathcal{L}_1\varphi_{a1} + \mathcal{L}_2\varphi_a = \sigma_0\varphi_{a2} + \sigma_1\varphi_{a1} + \sigma_2\varphi_a - \mu_1\varphi_{b1} - \mu_2\varphi_b \tag{30}$$

and similar equations for φ_{bi}.

4.2.2. Stabilization by friction at first order

The first-order corrections of the eigenvalue σ are obtained as solvability conditions of (29) by

$$\langle\varphi_a, \mathcal{L}_1\varphi_a\rangle = \sigma_1\langle\varphi_a, \varphi_a\rangle, \tag{31}$$

$$\langle\varphi_b, \mathcal{L}_1\varphi_a\rangle = -\mu_1\langle\varphi_b, \varphi_b\rangle, \tag{32}$$

where $\langle f, g\rangle \equiv (1/L)\int_0^L f(x)g(x)\,\mathrm{d}x$. In $\langle\varphi_a, \mathcal{L}_1\varphi_a\rangle$, the contributions from β immediately vanish by integration. We have, after integration by part

$$\langle\varphi_a, \mathcal{L}_1\varphi_a\rangle = -\lambda\langle v_a^2, W_0'''\bar{v}^{(1)}\rangle + r\langle v_a, \partial_x^{-2}v_a\rangle. \tag{33}$$

The first contribution to the right-hand side of (33) can be reduced to an integral over a single kink by summing the trigonometric factors arising from v_a^2:

$$\langle v_a^2, W_0'''\bar{v}^{(1)}\rangle = \frac{r}{\Lambda}\int W_0'''\bar{v}_r^{(1)}(\partial_x M_j)^2\,\mathrm{d}x. \tag{34}$$

Here j labels an arbitrary kink and the integral bounds do not need to be specified since $\partial_x M_j$ decays exponentially for both positive and negative x. This contribution is further transformed using

$$\int W_0'''\bar{v}_r^{(1)}(\partial_x M_j)^2\,\mathrm{d}x = \frac{1}{\lambda}\int \partial_x^{-1}\bar{v}^{(0)}\partial_x M_j\,\mathrm{d}x,$$

which is valid up to exponentially small errors. Finally the contribution is reduced to a nonlocal integral by part:

$$\frac{1}{\Lambda}\int \partial_x^{-1}\bar{v}^{(0)}\partial_x M_j\,\mathrm{d}x = \frac{1}{2\Lambda}\int_{x_j-(1/2)\Lambda}^{x_j+(1/2)\Lambda}\partial_x\bar{v}^{(0)}\partial_x^{-1}\bar{v}^{(0)}\,\mathrm{d}x = -\frac{1}{2}\Gamma^2 + \frac{2\Gamma^2}{\Lambda s}.$$

Combining this with (C.2) and (C.8), we obtain

$$\sigma_1 = -r\sin^2\frac{1}{2}\theta_m + \frac{4r}{\Lambda s}\left(1 + \cos^2\frac{1}{2}\theta_m\right)\left(1 - \frac{4}{\Lambda s}\cos^2\frac{1}{2}\theta_m\right)^{-1} + \mathrm{O}(\mathrm{e}^{-s\Lambda/2}). \tag{35}$$

In a similar way, we have

$$\langle\varphi_b, \mathcal{L}_1\varphi_a\rangle = -\lambda\langle v_a v_b, W_0'''\bar{v}^{(1)}\rangle + c_1\langle v_a, \partial_x^{-1}v_b\rangle - \beta\langle v_a, \partial_x^{-3}v_b\rangle. \tag{36}$$

The first term in the right-hand side of (36) vanishes after the trigonometric summation. Using (C.8) and (C.9) and (C.1)–(C.3), we obtain

$$\mu_1 = \left(-\frac{2c_1\Gamma^2}{\Lambda}t - \frac{\Gamma^2\Lambda}{8}t(1+t^2) + \frac{\pi^2\Gamma^2}{6s^2\Lambda}t\right)\left(\frac{\Gamma^2}{2}(1+t^2) - \frac{2\Gamma^2}{s\Lambda}\right)^{-1} + \mathrm{O}(\mathrm{e}^{-s\Lambda/2}), \tag{37}$$

or, retaining only the first three orders of the expansion:

$$\mu_1 = \beta\left(-\frac{\Lambda t(2+3t^2)}{12(1+t^2)} - \frac{t(1+2t^2)}{3s(1+t^2)^2} + \frac{4}{3\Lambda s^2}\frac{t^5}{(1+t^2)3}\right) + \mathrm{O}\left(\frac{\beta}{\Lambda^2}\right) \tag{38}$$

with $t = \tan\pi m/2N$.

It is interesting to notice that the nonlinear contribution $\langle v_a^2, U_0'''\bar{v}^{(1)} \rangle$ is destabilizing the stationary solution. However, the direct linear damping by friction remains larger and the total effect of friction is always stabilizing. Therefore, the m-mode perturbation to the stationary solution is stabilized by friction for

$$r > r_c = 512 \frac{\mathrm{e}^{-s\Lambda}}{\Lambda} s^3 \lambda \cos^2 \frac{\pi m}{2N} \tag{39}$$

at leading order.

The corresponding result when $\gamma \neq 0$ is given in (D.6). The mean advection decreases the value of friction necessary to stabilize a given wavenumber.

4.2.3. Stabilization by β-effect at second order

At second order in ε, σ_2 is solution of the solvability condition. Here we set r to zero for simplification as stabilization by r is already obtained at first order:

$$\langle \varphi_a, \mathcal{L}_1 \varphi_{a1} \rangle + \langle \varphi_a, \mathcal{L}_2 \varphi_a \rangle = \sigma_2 \langle \varphi_a, \varphi_a \rangle - \mu_1 \langle \varphi_a, \varphi_{b1} \rangle. \tag{40}$$

The second term on the left hand side of (40) expands as

$$\langle \varphi_a, \mathcal{L}_2 \varphi_a \rangle = -\lambda \langle v_a^2, W_0''' \bar{v}^{(2)} \rangle - \tfrac{1}{2} \lambda \langle v_a^2, W_0^{IV} (\bar{v}^{(1)})^2 \rangle. \tag{41}$$

The second term is $O(\beta^2 \Lambda^3)$ while the first term is $O(\beta^2 \Lambda^4)$ and dominates at leading order. This term can be transformed in the same way as above for $\langle \varphi_a, \mathcal{L}_1 \varphi_a \rangle$, leading to

$$\langle \varphi_a, \mathcal{L}_2 \varphi_a \rangle = -\frac{\lambda}{\Lambda} \int Q^{(1)} \partial_x^2 M_j \, \mathrm{d}x + O(\beta^2 \Lambda^3),$$

where $Q^{(1)}$ is the right-hand side for the second-order version of (7). After dropping out all contributions that vanish owing to the symmetries, we obtain

$$\langle \varphi_a, \mathcal{L}_2 \varphi_a \rangle = \frac{\beta^2}{\Lambda} \int \partial_x^{-3} \bar{v}_\beta^{(1)} \partial_x^2 M_j \, \mathrm{d}x + \frac{\lambda}{2\Lambda} \int W_0''' (\bar{v}^{(1)})^2 \partial_x^2 M_j \, \mathrm{d}x + O(\beta^2 \Lambda^3). \tag{42}$$

The second term on the right-hand side of (42) is negligible relatively to the first. This later can be calculated using

$$\frac{1}{\Lambda} \int \partial_x^{-3} \bar{v}_\beta^{(1)} \partial_x^2 M_j \, \mathrm{d}x = \frac{1}{2\Lambda} \int_{x_j - (1/2)\Lambda}^{x_j + (1/2)\Lambda} \partial_x^{-3} \bar{v}_\beta^{(1)} \partial_x^2 \bar{v}^{(0)} \, \mathrm{d}x = \frac{1}{2\Lambda} \int_{x_j - (1/2)\Lambda}^{x_j + (1/2)\Lambda} \partial_x^{-1} \bar{v}_\beta^{(1)} \bar{v}^{(0)}$$

and (11). We obtain

$$\langle \varphi_a, \mathcal{L}_2 \varphi_a \rangle = \frac{\beta^2 \Lambda^4 \Gamma^2}{92,160 \, s^2 \lambda} + O(\beta^2 \Lambda^3). \tag{43}$$

The other contributions in (40) involve φ_{a1} and φ_{b1}. These quantities can be approximated in the same way as $\bar{v}^{(1)}$ at distance from the kinks. We have

$$4s^2 \lambda \varphi_{a1} = -\lambda \partial_x^{-1} (W_0''' \bar{v}^{(1)} v_a) - c_1 \partial_x^{-1} \varphi_a + \beta \partial_x^{-3} \varphi_a - \mu_1 \partial_x^{-2} \varphi_b \tag{44}$$

and a similar expression for φ_{b1}. Then, after some algebra and dropping the terms which do not contribute to the leading order, we have

$$4s^2 \lambda \langle \varphi_a, \mathcal{L}_1 \varphi_{a1} \rangle = c_1^2 \langle v_a, \partial_x^{-2} v_a \rangle + \beta^2 \langle v_a, \partial_x^{-6} v_a \rangle - 2\beta c_1 \langle v_a, \partial_x^{-4} v_a \rangle - \mu_1 \beta \langle v_a, \partial_x^{-5} v_b \rangle$$
$$+ \mu_1 c_1 \langle v_a, \partial_x^{-3} v_b \rangle + O(\beta^2 \Lambda^3).$$

Using the results of Appendix C, we obtain

$$\langle \varphi_a, \mathcal{L}_1 \varphi_{a1} \rangle = -\frac{\beta^2 \Gamma^2 \Lambda^4}{92,160 \, s^2 \lambda}(1 + 6t^2 + 15t^4) + O(\beta^2 \Lambda^3).$$

and

$$\langle \varphi_a, \varphi_{b1} \rangle = -\frac{\beta \Gamma^2 \Lambda^3}{4608 \, s^2 \lambda}(t + 3t^3) + O(\beta \Lambda^2).$$

Finally

$$\sigma_2 = -\frac{\beta^2 \Lambda^4}{69,120 \, s^2 \lambda} \frac{t^2(4 + 9t^2)}{(1 + t^2)^2} + O(\beta^2 \Lambda^3). \tag{45}$$

The contribution from r^2 is a correction to the first-order stabilization obtained in σ_1. The β term does not appear at first order and is stabilizing in (45). Though the effect is small, it increases algebraically with Λ while the nonlinear coupling of kinks decreases exponentially in (18). Therefore, if $r = 0$, stabilization of the m-mode perturbation to the stationary solution is obtained at leading order for

$$\beta > \beta_c = \left(35,389,440 \frac{\mathrm{e}^{-s\Lambda}}{\Lambda^5} s^5 \lambda^2 \frac{1}{4 + 9t^2} \right)^{1/2}. \tag{46}$$

The condition is the most restrictive for $m = 1$, that is $t = \tan \pi/(2N)$.

4.3. Stability of β-CH equation with finite radius of deformation

In this case $\mathcal{L}_1$ and $\mathcal{L}_2$ are modified as

$$\mathcal{L}_1 = \lambda \partial_x W_0''' \bar{v}^{(1)} \partial_x + c_1 \partial_x - (\beta + c_1 S^2) \partial_x^{-1} - r, \tag{47}$$

$$\mathcal{L}_2 = \lambda \partial_x (W_0''' \bar{v}^{(2)} + \tfrac{1}{2} U_0^{IV} \bar{v}^{(1)^2}) \partial_x + c_2 (\partial_x - S^2 \partial_x^{-1}). \tag{48}$$

At first order in ε, the imaginary part of the eigenvalue is

$$\mu_1 = -c_1 \frac{\langle v_a, \partial_x^{-1} v_b \rangle}{\langle vfb, \partial_x^{-2} \varphi_b \rangle} + (\beta + S^2 c_1) \frac{\langle v_a, \partial_x^{-3} v_b \rangle}{\langle vfb, \partial_x^{-2} \varphi_b \rangle} = -\frac{4\beta t (2 + 3t^2)}{\Lambda S^2 (1 + t^2)} + O\left(\frac{\beta}{\Lambda^2}\right) \tag{49}$$

At second order in ε, σ_2 is still given by (40). The contribution $\langle \varphi_a, \mathcal{L}_2 \varphi_a \rangle$ is now

$$\langle \varphi_a, \mathcal{L}_2 \varphi_a \rangle = \frac{\beta(\beta + c_1 S^2)}{\Lambda} \int \partial_x^{-3} \bar{v}_\beta^{(1)} \partial_x^2 M_j \, \mathrm{d}x + O\left(\frac{\beta^2}{\Lambda}\right).$$

After integration by part and using (14), we obtain

$$\langle \varphi_a, \mathcal{L}_2 \varphi_a \rangle = -\frac{\beta^2 \Gamma^2}{40 \, s^2 S^4 \lambda} + \left(\frac{\beta^2}{\Lambda}\right).$$

Similarly, we have

$$\langle \varphi_a, \mathcal{L}_1 \varphi_{a1} \rangle = -\frac{\beta^2 \Gamma^2}{40 \, s^2 S^4 \lambda}(1 + 6t^2 + 15t^4) + O\left(\frac{\beta^2}{\Lambda}\right), \qquad \langle \varphi_a, \varphi_{b1} \rangle = -\frac{\Gamma^2 \Lambda}{96 \, s^6 S^2 \lambda} t(1 + 3t^2) + O(1).$$

Finally, we obtain σ_2 as

$$\sigma_2 = -\frac{\beta^2}{30\,s^2 S^4 \lambda} \frac{3 + 7t^2 + 9t^4}{(1 + t^2)^2} + \mathrm{O}\left(\frac{\beta^2}{\Lambda}\right). \tag{50}$$

The stability cross-over for β is now

$$\beta_c = \left(15,360\,s^5 S^4 \lambda^2 \frac{3 + 7t^2 + 9t^4}{t^2} \frac{\mathrm{e}^{-s\Lambda}}{\Lambda}\right)^{1/2}. \tag{51}$$

Therefore, the stabilizing effect of β is much reduced compared to that with infinite radius of deformation.

All the perturbative calculations of Sections 3 and 4 have been checked with Mathematica.

5. Numerical results

The analytic results established in Section 4 are valid in the double limit of small ϵ and large Λ. These asymptotic results are complemented and compared with three types of numerical calculations: (i) numerical solution of the perturbative problem for several values of Λ, (ii) direct numerical simulation of the Cahn–Hilliard equation in the Fourier space and (iii) direct stability calculation.

5.1. Numerical solution of the perturbative problem

We relax here the hypothesis on the large value of Λ by solving numerically the perturbative equations for $\bar{v}^{(1)}$, $\bar{v}^{(2)}$, φ_{a1} and φ_{b1}, and numerically evaluating the solvability conditions.

The calculation is performed according to the following algorithm:

(1) The basic solution $\bar{v}^{(0)}$ is defined by the approximate form given in Appendix A.
(2) The inverse derivatives $\partial_x^{-1}\bar{v}^{(0)}$, $\partial_x^{-2}\bar{v}^{(0)}$ and $\partial_x^{-3}\bar{v}^{(0)}$ are calculated by Fourier transform and tabulated to obtain $Q^{(0)}$.
(3) c_1 is calculated by discrete evaluation of (8).
(4) (7) is discretized as a tridiagonal problem and solved for $\bar{v}_\beta^{(1)}$ and $\bar{v}_r^{(1)}$.
(5) $Q^{(1)}$ is built in the same way as $Q^{(0)}$ from the inverse derivatives of $\bar{v}_\beta^{(1)}$ and $\bar{v}_r^{(1)}$.
(6) $\bar{v}^{(2)}$ is calculated by inverting a tridiagonal discretized problem.
(7) The eigenvectors v_a and v_b are defined using (19) and (20).
(8) φ_a and φ_b are calculated by Fourier transform and tabulated.
(9) σ_1 and μ_1 are calculated according to (25), (31) and (32).
(10) φ_{a1} and φ_{b1} are obtained using (29) and solving a tridiagonal discretized problem.
(11) σ_2 is obtained from (25), (26) and (40).

This algorithm admits $\mathrm{O}(\mathrm{e}^{-s\Lambda/2})$ errors, but all the steps generating errors of algebraic order in the asymptotic expansion are here solved numerically. The implementation has been done as a Mathematica notebook available from the authors. The number of grid points and Fourier modes has been adjusted as a function of L and N in order to provide at least three digits of accuracy in the results. The symmetries have been exploited to distinguish the solutions and reduce the number of points.

5.2. Numerical solution of the complete Cahn–Hilliard equation

We have done numerical simulations of the complete Cahn–Hilliard equation (1) for the case $\gamma = S = 0$. For practical convenience, the spatial period has been kept fixed to 2π by rescaling x as $x \rightarrow px$, hence $L = 2\pi p$. The complete Cahn–Hilliard equation then reads

$$\partial_t v = \frac{\lambda}{p^2} \partial_x^2 W'(v) - \frac{\lambda}{p^4} \partial_x^4 v - p\beta \partial_x^{-1} v - rv. \tag{52}$$

Since Fourier modes are discretized by the periodicity condition, the number n of unstable modes for $v = 0$ is the integer part of $p(2/3)^{1/2}$.

5.2.1. Time-dependent simulations

The simulations are performed using a standard semi-spectral method where the number of retained real Fourier modes is 256. The collocation grid in the spatial domain has 512 points in order to fully remove the aliasing due to the cubic term in (52). We have checked that using higher resolution does not modify the results within the explored parameter range. The temporal integration is performed with an Adams–Bashforth second-order scheme. Initial conditions are a random white noise in the spatial domain. We have made a large number of runs by varying the initial conditions (changing the seed of the pseudo-random number generator and the amplitude of the noise), the values of r and n.

Section 4 shows the existence of multiple stable solutions induced by β and friction but does not provide indications about the attraction basins of these solutions. In the inverse cascade of the standard Cahn–Hilliard equation, the interaction of a pair of neighboring kink and antikink scales as $\exp(-s\Delta x)$, where Δx is the distance between the kink and the antikink (see Appendix B). When friction r is just above the critical value $r_c(N)$ stabilizing the solution with N pairs, we may conjecture that the stabilizing effect is of the order $O((r - r_c(N))\delta x)$, where δ_x is the departure of a kink from its equilibrium position (this is clear from the shape of the eigenmodes v_a and v_b (cf. Section 4.1)). This effect, however, cannot extend very far in δx as the attraction to the next antikink grows as $\exp(s\delta x)$. Moreover, the time-dependent solutions do not need to pass in the vicinity of the N-pair fixed point during the cascade of kink–antikink annihilations. Therefore, we expect that the fraction of the solutions halting on the N-pair stable state will be small in the vicinity of the critical r_c and will be significant only when the stabilizing effect is felt over a distance of order Λ. Once this is obtained, very few solutions should jump to lower N states.

Fig. 3 shows how the inverse cascade evolves as a function of r for the same initial conditions, with the corresponding steady states shown in Fig. 4. The final state wavenumber increases with r and stays bounded by the value of the most unstable eigenmode of the Kolmogorov flow $k = (2/3)^{1/2}n$ which is the unique mode excited when r approaches r_0. The total energy calculated as the sum of the various energies $E(k)$ of the single modes k, decreases as the friction increases.

Fig. 5 compares the halting of the inverse cascade by friction and by β effect for the same initial conditions. It is apparent from Fig. 3 that friction simply halts the cascade by stabilizing one of the intermediate steps. Here, the effect of the β-term is more complex: oscillatory transients are excited and, paradoxically, the cascade is accelerated. In Fig. 5 the transitions to $N = 3$ and to $N = 2$ occur much earlier than in the absence of β. Other examples can be found in [11,18]. In the final state, the β effect breaks the symmetry between the kinks and the antikinks which is preserved by friction.

5.2.2. Numerical stability calculations

In order to compare the results from the analytic and numerical perturbation approaches to the direct simulation of the complete Cahn–Hilliard equation, we have developed a direct analysis of stability by the same technique as for
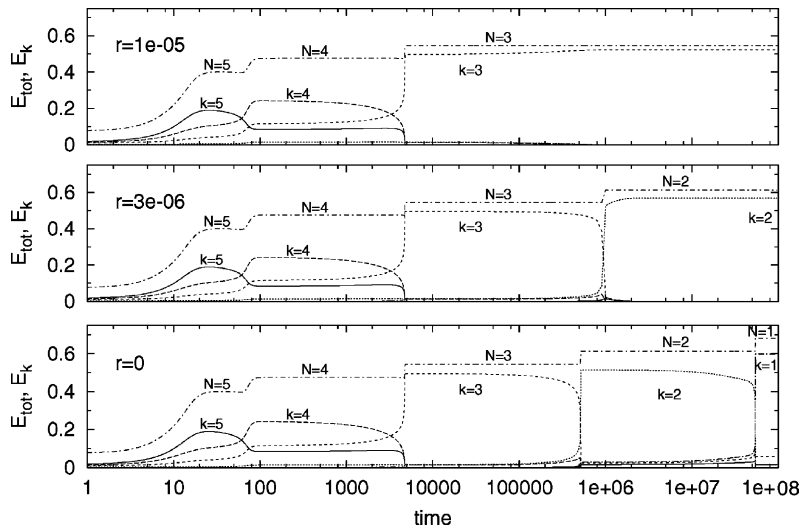
Fig. 3. Temporal evolution of the energies $E(k)$ of the Fourier modes and their sum E_{tot}. The three shown cases, are for $r = 0$, $r = 3 \times 10^6$ and $r = 10^5$, with $\beta = 0$, $n = 10$ and the same realization of white noise as initial condition. For $r = 0$ the inverse cascade is complete to $N = 1$; for the other values the cascade stops, respectively, on $N = 2$ and on $N = 3$. Note that E_{tot} is constant between two annihilation events. Increasing r further enables to stop the cascade on larger N configurations (not shown).

the time-dependent simulations. The core of this analysis is to calculate the Jacobian matrix of the right-hand side of (52) linearized around a given state v, with respect to each of the Fourier component. This is done by differentiating (52) and calculating the columns of the Jacobian matrix by the semi-spectral method applied to the differentiated equations for each Fourier component.

The stability calculation is performed as follows. First an estimate of the stationary solution based on Appendix A is refined by a Newton–Raphson algorithm which usually converges within a few steps. The degeneracy due to
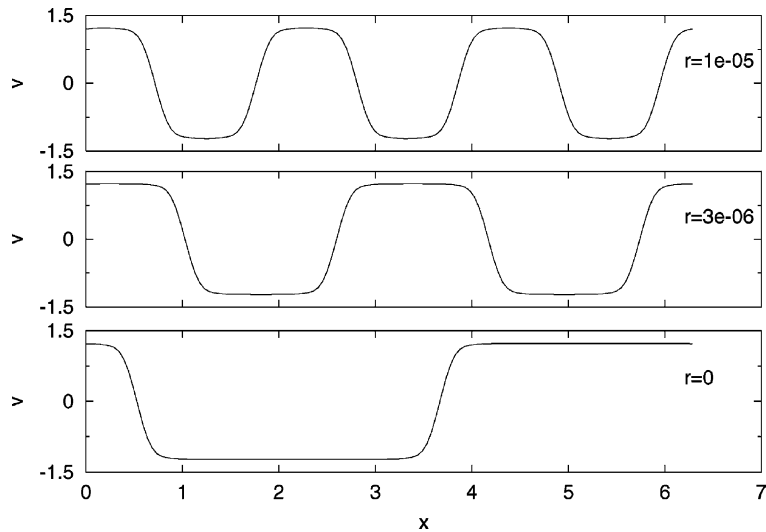

Fig. 4. The corresponding asymptotic velocity profile for the three cases presented in Fig. 3. Note that the kinks–antinkinks pairs are equidistant, unlike the $N = 2$ or $N = 3$ configurations of Fig. 1 which are only metastable.
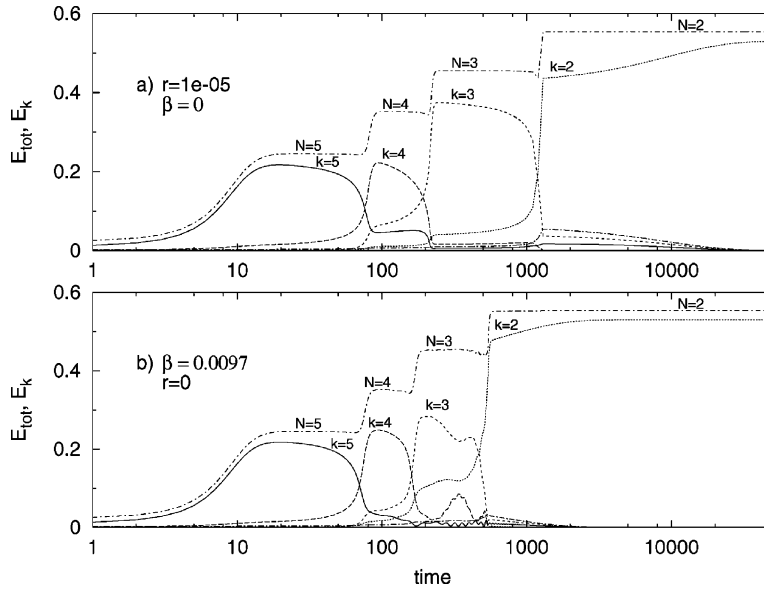
Fig. 5. Comparison between two temporal evolution of E_{tot} and $E(k)$, for the same initial conditions and for very similar final solutions with same N and final energy $E_{\text{tot}} \simeq 0.5535$. Top: $r = 10^{-5}$ and $\beta = 0$. Bottom: $r = 0$ and $\beta = 9.7 \times 10^{-3}$.

the x-invariance of the complete Cahn–Hilliard equation is removed by setting to zero the imaginary part of the dominating Fourier mode and removing the corresponding row and line from the Jacobian matrix. In the case $\beta \neq 0$, the solution is stationary in a frame traveling at a velocity c. This phase velocity is treated as an additional unknown increasing the dimension of the Jacobian matrix by 1. The stability of this numerical solution is then found by finding the eigenvalues and the eigenmodes of the Jacobian matrix using a standard QR algorithm from LINPACK. In this procedure, we find both the slow components associated to kink dynamics and the highly damped modes associated with fast relaxing transients. The conditioning of the eigenvalue problem gets very bad as Λ increases as a result of the large separation between slow and fast eigenvalues, thus limiting the parameter range for the numerical calculation of stability. There is enough overlap, though, with the validity domain of the perturbative theory to provide detailed comparison. The number of Fourier modes used in this analysis has been 128, 256 or 384, depending on the values of L and N.

5.3. Comparison of stability results

Table 1 compares the critical values of friction and β estimated from the analytic perturbative expansion, the numerical solution to the perturbation problem and the numerical stability analysis. In the numerical stability analysis the value of the parameter is adjusted by dichotomy from two values bracketing the transition. There is an excellent agreement between the three values of critical friction when Λ is large. At the largest values, however, the QR algorithm fails to converge and no results are obtained for the numerical stability. When Λ is not large, that is when the kinks are not distant enough to neglect the contribution of $O(e^{-s\Lambda/2})$, significant discrepancies occur between the different estimates. We see from the table that this occurs when $e^{-s\Lambda/2} \gtrsim 3 \times 10^{-2}$.

There is also an excellent agreement between β_c^{pert} and β_c^{num} for the same range of Λ values as for r_c. The analytical prediction (46), however, provides only an order of magnitude and is wrong by at least a factor 2 when the two other quantities agree by four digits. The reason is that the error in (46) depends algebraically on Λ unlike the

Table 1

Critical values of friction and β as a function of the number of unstable modes n (or equivalently the size of the domain $L = n(3/2)^1/2$) and the wavenumber N of the stationary solution[a]

n	N	$e^{-s\Lambda/2}$	r_c^{an}	r_c^{pert}	r_c^{num}	β_c^{an}	β_c^{pert}	β_c^{num}
7	2	4×10^{-4}	6.8478×10^{-7}	6.8484×10^{-7}	6.848×10^{-7}	1.06×10^{-4}	2.0522×10^{-4}	2.0523×10^{-4}
	3	6×10^{-3}	2.7469×10^{-4}	2.7705×10^{-4}	2.779×10^{-4}	5.88×10^{-3}	1.6329×10^{-2}	1.6385×10^{-2}
	4	2×10^{-2}	5.5655×10^{-3}	5.9149×10^{-3}	6.147×10^{-7}	5.58×10^{-2}	0.216	0.222
	5	5×10^{-2}	3.4908×10^{-2}	3.9614×10^{-2}	5.139×10^{-2}	0.260	1.473	1.379
20	2	2×10^{-10}	6.8832×10^{-20}	6.8825×10^{-20}	NA	3.93×10^{-12}	4.82×10^{-22}	NA
	3	4×10^{-7}	4.1846×10^{-13}	4.1847×10^{-13}	NA	2.50×10^{-8}	3.42×10^{-8}	NA
	4	2×10^{-5}	1.0438×10^{-9}	1.0439×10^{-9}	1.009×10^{-9}	2.41×10^{-6}	3.780×10^{-6}	3.716×10^{-6}
	5	1×10^{-4}	1.1756×10^{-7}	1.1756×10^{-7}	1.1751×10^{-7}	4.23×10^{-5}	7.782×10^{-5}	7.782×10^{-5}
	6	6×10^{-4}	2.8135×10^{-6}	2.8143×10^{-6}	2.8144×10^{-6}	3.13×10^{-4}	6.858×10^{-4}	6.858×10^{-4}
	7	2×10^{-3}	2.7738×10^{-5}	2.7778×10^{-5}	2.7795×10^{-5}	1.40×10^{-3}	3.706×10^{-2}	3.710×10^{-2}
	8	4×10^{-3}	1.5681×10^{-4}	1.5750×10^{-4}	1.580×10^{-4}	4.52×10^{-3}	1.468×10^{-2}	1.479×10^{-2}
	9	7×10^{-3}	6.1103×10^{-4}	6.1582×10^{-4}	6.242×10^{-4}	1.18×10^{-2}	4.676×10^{-2}	4.827×10^{-2}
	10	1×10^{-2}	1.8329×10^{-3}	1.8416×10^{-3}	1.921×10^{-3}	2.68×10^{-2}	0.124	0.138
	11	2×10^{-2}	4.5418×10^{-3}	4.4508×10^{-3}	4.965×10^{-3}	5.24×10^{-2}	0.287	0.373
	12	2×10^{-2}	9.7452×10^{-3}	8.9096×10^{-3}	1.135×10^{-2}	9.58×10^{-2}	0.551	1.01
	13	3×10^{-2}	1.8708×10^{-2}	1.4927×10^{-2}	2.392×10^{-2}	0.164	0.951	2.11

[a] The columns r_c^{an} and β_c^{an} show the analytical predictions given by (39) and (46) for $m = 1$. The columns r_c^{pert} and β_c^{pert} show the critical values obtained by numerically solving the perturbation problem as indicated in Section 5.1, again for $m = 1$. The columns r_c^{num} and β_c^{num} show the critical values obtained from the direct numerical stability study of the complete Cahn–Hilliard equation, as indicated in Section 5.2.2.

error in (39) where the error exhibits an exponential dependence. Very large values of Λ are required to make (46): for $n = 200$ and $N = 5$, we obtain $\beta_c^{pert} = 2.24 \times 10^{-42}$ and $\beta_c^{num} = 2.35 \times 10^{-42}$, while for $N = 2$ we obtain $\beta_c^{pert} = 1.842 \times 10^{-101}$ and $\beta_c^{num} = 1.808 \times 10^{-101}$. This difficulty with β is entirely due to the need to solve completely the perturbation at order 1. The phase speed c_1 and the frequency μ_1, which are obtained as solvability conditions at order 1, are known with the same accuracy as r_c, as can be checked in Table 2.

5.4. Comparison of stability properties and time-dependent solutions

In order to assess the distribution of final states among the multiple stable steady states we have performed ensemble simulations for a number of values of r and β. Each numerical integration of the time-dependent numerical model described in Section 5.2.1 is characterized by n, r, β and the initial condition. We choose for this a white noise with amplitude A in the spatial domain. For each value of the parameters and for two values of the amplitude, $A = 0.1$ and $A = 1.0$, we performed an ensemble of 100 independent simulations by varying the seed of the random number generator. After some time, all simulations converge to a final stationary or uniformly traveling state (if $\beta = 0$ or $\beta \neq 0$, respectively). The nonconvergent cases are due to fast transients leading to nonlinear numerical instabilities.

Table 3 shows the dependence on r when $\beta = 0$ and $n = 20$. The distribution of final states agree qualitatively with the analysis presented in Section 5.2.1. Stationary states associated to given value of N are only reached for r larger than the critical value $r_c(N)$. The proportion of solutions reaching these stationary states is about 15% for $A = 0.1$ and 10% for $A = 1.0$ when $r/r_c(N) \approx 3$. This proportion grows rapidly as r increases further while the number of states reaching solutions with smaller N falls dramatically. In practice, it is difficult to find values of r where more than three steady states are obtained. It is also visible that larger amplitude of the initial conditions favor smaller final N and more dispersion of the final states.

Table 2
Values of the phase speed of the basic solution and the frequency of the $m = 1$ mode as a function of n and N[a]

n	N	c_1^{an}/β	c_1^{pert}/β	c^{num}/β	μ_1^{an}/β	μ_1^{pert}/β	μ^{num}/β
7	2	−17.6492	−17.6492	−17.649	−6.01296	−6.01298	−6.0127
	3	−8.05199	−8.0485	−8.0486	−2.21915	−2.22148	−2.222
	4	−4.61026	−4.57267	−4.5730	−1.16117	−1.18408	−1.1876
	5	−3.11049	−2.93650	−2.9368	−0.63701	−0.73943	−0.74685
20	2	−133.043	−133.043	−133.04	−16.4572	−16.4571	NA
	3	−60.8209	−60.8209	−60.821	−5.86179	−5.86179	NA
	4	−35.0024	−35.0024	−35.002	−3.08063	−3.08063	−3.0806
	5	−22.8122	−22.8122	−22.812	−1.92726	−1.92726	−1.9273
	6	−16.0670	−16.0669	−16.067	−1.33119	−1.33123	−1.3312
	7	−11.9316	−11.9310	−11.931	−0.979702	−0.979894	−0.97994
	8	−9.20895	−9.20716	−9.2074	−0.753012	−0.753716	−0.75386
	9	−7.32184	−7.31636	−7.3170	−0.596714	−0.59863	−0.59900
	10	−5.96367	−5.95021	−5.9514	−0.482911	−0.487182	−0.48791
	11	−4.95971	−4.93139	−4.9335	−0.395862	−0.404176	−0.40547
	12	−4.20511	−4.15177	−5.1550	−0.325842	−0.340601	−0.34263
	13	−3.63500	−3.54226	−3.5452	−0.266160	−0.290808	−0.2927

[a] The columns $c1^{an}/\beta$ and μ_1^{an}/β show the analytical predictions given by (8 and 37). The columns c_1^{pert}/β and μ_1^{pert}/β show the values obtained by numerically solving the eigenvalue problem. μ_1^{an} and μ_1^{pert} are calculated for $m = 1$. The columns c^{num}/β and μ^{num}/β show the values obtained from the direct numerical stability study of the complete Cahn–Hilliard equation near the critical value of β. μ^{num} is the frequency of the critical mode.

Table 4 shows the corresponding results as a function of β when $r = 0$. They are qualitatively similar to the precedings although up to seven different final states are now observed for $\beta = 1$.

5.5. Attracting solutions and Lyapunov functional

In the presence of friction, the Lyapunov functional is

$$F = \int_0^L \left(\frac{r}{2}\psi^2 + \frac{\lambda}{2}(\partial_x v)^2 + \lambda W(v) \right) dx, \tag{53}$$

where we have set $\gamma = S = 0$ for simplicity. By using the same approximations as in Section 3, we obtain

$$F = \Gamma^2 L \left\{ r \left(\frac{\Lambda^2}{96} + \frac{11/12\pi - 1}{4s^2} + \frac{\zeta(3)}{4\Lambda s^2} \right) + \frac{8\lambda s}{\Lambda} - \frac{\lambda s^2}{2} \right\}. \tag{54}$$

Manfroi and Young [5] observed that minimizing F with respect to Λ yields $r \sim \Lambda_{\min}^{-3}$ and suggested that final steady states should satisfy this scaling in the presence of friction. From (54), we have

$$\Lambda_{\min} = \left(\frac{128s}{r} + \frac{12\zeta(3)}{s^3} \right)^{1/3}. \tag{55}$$

It is easy to check that this wavelength is always larger than the critical value provided by the stability condition (39). In a finite domain, it is necessary to find the minimum of F over the discrete set of the steady states. We have performed this calculation for $n = 20$ and all the values of friction in Table 3. Both (54) and the numerical calculation of F from the steady state calculated in Section 5.2.2 with (53) provide the same wavenumber N_m minimizing F. This wavenumber is indicated in Table 3 to be compared with the critical N bounding the stability domain and the distribution of final steady states. It is clear that the solutions initialized with a white noise do not

Table 3
Distribution of solutions as a function of N for $n = 20$, $\beta = 0$ and increasing values of r[a]

r_c	r	N_m	N	$A = 0.1$	$A = 1.0$
2.81×10^{-6}			6		
	10^{-5}	1	4	4%	19%
			5	81%	71%
			6	15%	10%
	1.78×10^{-5}	1	4	1%	8%
			5	57%	69%
			6	42%	23%
2.78×10^{-5}			7		
	3.16×10^{-5}	1	4	0%	1%
			5	44%	52%
			6	56%	41%
	5.62×10^{-5}	1	5	23%	30%
			6	74%	67%
			7	3%	3%
	10^{-4}	1	5	9%	16%
			6	76%	75%
			7	15%	9%
1.57×10^{-4}			8		
	1.78×10^{-4}	2	5	1%	2%
			6	50%	65%
			7	49%	33%
	3.16×10^{-4}	2	6	18%	34%
			7	75%	64%
			8	7%	2%
	5.62×10^{-4}	2	6	1%	19%
			7	63%	62%
			8	36%	2%
6.16×10^{-4}			9		
	10^{-3}	3	6	0%	6%
			7	29%	40%
			8	69%	54%
			9	2%	0%
	1.78×10^{-3}	3	7	1%	20%
			8	74%	71%
			9	25%	9%
1.84×10^{-3}			10		
	3.16×10^{-3}	4	7	0%	3%
			8	26%	57%
			9	68%	69%
			10	6%	
4.45×10^{-3}			11		
	5.62×10^{-3}	5	8	2%	20%
			9	66%	70%
			10	32%	10%
8.90×10^{-3}			12		
	10^{-2}	6	8	0%	3%
			9	20%	51%
			10	66%	45%
			11	14%	1%
1.49×10^{-2}			13		
	1.78×10^{-2}	7	9	1%	9%
			10	33%	59%
			11	62%	32%
			12	4%	0%
	3.16×10^{-2}	8	10	3%	17%
			11	48%	59%
			12	48%	23%
			13	1%	1%

[a] The statistics is calculated out of an ensemble of 100 cases for each value of r and A. The cases are obtained by varying the seed of the random generator. The fifth and the sixth columns show the percentages of solutions ending on the stable N-pair solutions with N in the fourth column. The first column gives the critical linear stability r_c as a function of N (same line in the fourth column), provided by the numerical solution to the perturbative problem (see Section 3). The third column gives for each value of r the steady state wavenumber with the minimum value of the Lyapunov functional.

Table 4
Same as Table 3 but for the distribution of solutions as a function of N for $n = 20$, $r = 0$ and increasing values of β

β_c	β	N	$A = 0.1$	$A = 1.$
7.78×10^{-5}		5		
	10^{-4}	3	12%	13%
		4	85%	87%
		5	3%	0%
6.86×10^{-4}		6		
	10^{-3}	4	17%	36%
		5	82%	63%
		6	1%	1%
3.71×10^{-3}		7		
	10^{-2}	5	0%	2%
		6	74%	68%
		7	26%	30%
1.47×10^{-2}		8		
4.68×10^{-2}		9		
	0.1	7	2%	10%
		8	56%	78%
		9	42%	12%
0.124		10		
0.288		11		
0.551		12		
	1.0	7	0%	1%
		8	0%	2%
		9	0%	17%
		10	16%	26%
		11	65%	46%
		12	18%	8%
		13	1%	0%

reach N_m but cluster over a few wavenumbers near the critical N as described in Section 5.4. This suggest that the attraction basin of the most stable solution is indeed very small in the phase-space of the solutions.

6. Summary and conclusion

We have investigated the stabilization induced by friction and β effect in the inverse cascade of the large-scale instability of the Kolmogorov flow. This problem has been treated by solving the unidimensional complete Cahn–Hilliard equation using both numerical simulations and perturbation techniques.

In the standard Cahn–Hilliard equation, the kinks and antikinks are coupled by interactions decreasing exponentially as a function of their separation. The number of kinks decreases with time and their average separation increases as a result of the inverse cascade. Therefore the Cahn–Hilliard coupling also decreases with time.

The basic effect of friction is to damp uniformly the motion of the kinks and antikinks. Nonlinear effects due to the deformation of the kinks tend to reduce this damping but cannot invert it. When the separation is large enough, the damping overcomes the destabilizing Cahn–Hilliard coupling halting the inverse cascade before it reaches the gravest mode. The dependence of the critical friction r_c upon the kink separation $\Lambda/2$ scales as $r_c \sim (\mathrm{e}^{-s\Lambda}/\Lambda)$. The perturbative approach yields a very accurate analytical expression of r_c because the leading contribution to $r_c\,\mathrm{e}^{s\Lambda}$, which is algebraic in Λ, can be obtained exactly leaving out only terms which are exponentially small in Λ.

Stabilization by β-effect is more complex. It does not contribute to the linearization of Cahn–Hilliard equation around a steady state and appears only at the second order of the perturbative expansion in β. As the first-order step

of the perturbation expansion is only solved for the leading contribution in a $1/\Lambda$ expansion, the analytic expression of the critical β_c is fairly inaccurate when compared to numerical solution of the perturbative problem or to direct stability calculations. Its scaling $\beta_c \sim (e^{-s\Lambda}/\Lambda^5)^{1/2}$ is, however, correctly predicted.

The presence of a finite radius of deformation $1/S$ slows down the fastest Rossby waves and provides less efficient stabilization by the β effect. The critical β_c then scales as $\beta_c \sim (e^{S^4-s\Lambda}/\Lambda)^{1/2}$.

In the presence of mean advection, as in Ref. [5], the eastward jets are narrow and strong while the westward jets are broad and slow. The critical value of friction is reduced (see (D.6)) and scales as $r_c \sim (e^{-s\Lambda(1-\gamma/\Gamma)}/\Lambda)$.

Stabilization is demonstrated near the modified steady states of the Cahn–Hilliard equation. The attraction basin of these steady states depends on the stability of time-dependent solutions and has been investigated numerically. The results suggest a fairly simple pattern where, for most values of the parameters, the phase-space is filled by the attraction basins of only two or three stationary solutions. The boundary of these basins might be very complicated, even fractal. The most attracting solution has a wavenumber smaller than the critical wavenumber by one to two units and larger than the wavenumber corresponding to the minimum of the Lyapunov functional (when this is defined later). It is quite possible that the addition of external stochastic forcing to the dynamics would help the solutions to jump over the barriers between the different attraction basins and reach the minimum of the Lyapunov functional. This has not yet been investigated.

We have observed in the numerical simulations of the pure Cahn–Hilliard equation that the inverse cascade does not always begin by the most unstable state $N = k_m$; however it is in principle always possible to stop the cascade at such a state by enhancing the friction. The same is not true for β, which is not always able to stop the cascade at the scale corresponding to the most unstable state. As already noticed, β dispersive effect is more complex than friction effect. While the inverse cascade prior to the halting by friction does not differ from the pure Cahn–Hilliard case, the β effect is generally accelerating the cascade before halting. We speculate that this is due to the propagation of fast Rossby waves superimposed to the kinks and increasing their coupling.

The scaling of the critical β_c also differs from the scaling $\beta_c \sim \Lambda^{-3}$ which would arise from standard phenomenology [1] by balancing the nonlinear and the dispersive term in (1). The reason lies in the suppression of nonlinearities in the slow manifold for solutions of the complete Cahn–Hilliard equation once the initial transients have been dissipated. In more realistic two-dimensional or quasigeostrophic flows, the presence of strong dominating jets and/or coherent eddies is similarly inducing a reduction of nonlinearities with respect to a plain dimensional estimate. This is why the prediction of a k^{-3} energy spectra [19] is usually not observed in forced two-dimensional flows [20] with the possible exceptions of the smallest quasi-passive scales of the motion.

Acknowledgements

Appendix A. Approximate solution of the Cahn–Hilliard equation

The stationary form of the Cahn–Hilliard equation $\partial_x^2 v - U'(v) = 0$ can be recast as

$$\partial_x U = \tfrac{1}{2}\partial_x(\partial_x v)^2 \tag{A.1}$$

from which the solution is obtained by quadrature. By integrating (A.1) once, we obtain

$$U = \tfrac{1}{2}(\partial_x v)^2 - C, \tag{A.2}$$

where C is a constant which determines the value of $\partial_x v$ on the kinks and the periodicity of the solution. For the single-kink solution (5), we have $C = (1/2)s^2 \Gamma^2$ and the asymptotic value of U is $-C$. Let us now assume

$$C = \tfrac{1}{2}s^2 \Gamma^2(1 - \mu),$$

where μ is assumed a small perturbation and try a solution under the form

$$v = \Gamma \tanh sx + \mu \tilde{v}. \tag{A.3}$$

By replacing in (A.2) and expanding, we obtain, at first order in μ:

$$2\partial_x \tilde{v} = -4s\tilde{v} \tanh sx - \Gamma s \cosh^2 sx. \tag{A.4}$$

This equation can be solved as

$$\tilde{v} = -\frac{\Gamma}{16}\left((3 + \cosh^2 sx)\tanh sx + \frac{3sx}{\cosh^2 sx}\right), \tag{A.5}$$

where the condition $\tilde{v}(0) = 0$ has been used. We can relate μ to the period of the solution by using $\partial_x v = 0$ for $x = \Lambda/4$, leading to

$$\mu\left\{\frac{1}{8}s\Gamma\left(\tanh^2 sx(3 + 2\cosh^2 sx) + \frac{3s\tanh sx}{\cosh^2 sx}\right) - \frac{1}{2}\Gamma s \cosh^2 sx\right\} + s\frac{s\Gamma}{\cosh^2 sx} = 0. \tag{A.6}$$

When Λ is large the main contribution is

$$\mu = 64\,\mathrm{e}^{-s\Lambda}. \tag{A.7}$$

Comparison with numerical solutions of (1) shows that (A.3) with (A.5) and (A.7) approximates periodic stationary to less than 0.2% for $\Lambda > 10$. One can build a solution over the whole domain by using (A.3) over contiguous intervals containing a kink matched at mid-distance between adjacent kinks. The approximate solution is continuous and the discontinuity of its derivative at matching points is $\mathrm{O}(\exp(-s|x_{AK} - x_K|))$ where $|x_{AK} - x_K|$ is the distance between adjacent kinks.

Appendix B. Kink motion in the Cahn–Hilliard equation

This Section is adapted from Kawasaki and Ohta [12] and corrects one error found in that paper.

We assume that the solution is a combination of kinks which are individually described by (5). As $\partial_x^2 M_\ell(x)$ and $W'(M_\ell)$ decay rapidly away from $x = x_\ell$, the solution in the vicinity of the jth kink is the sum of $M_j(x)$ and small contributions from adjacent kinks which are the small deviations from their asymptotic values. We write

$$v(x, t) = M_j(x) + \tilde{v}_j(x, t), \tag{B.1}$$

where $\tilde{v}_j$ is small in the vicinity of the jth kink, but takes finite value at large distance. A valid expression in the vicinity of neighboring kinks is

$$\tilde{v}_j(x, t) = \sum_{\ell < j}(M_\ell(x) - M_\ell(+\infty)) + \sum_{\ell > j}(M_\ell(x) - M_\ell(-\infty)), \tag{B.2}$$

where $M_\ell(+\infty)$ and $M_\ell(-\infty)$ are the asymptotic values at infinity for the basic kink profile. Here we assume that kinks and antikinks alternate (i.e. $\epsilon_j \epsilon_{j+1} = -1$), and that they are numbered from 0 to $2N - 1$ within the periodic interval $[0, L]$. The time dependence is entirely contained within the positions of the kinks $\{x_j(t)\}$.

The temporal evolution of the solution is then given by

$$\partial_t v(x, t) = -\sum_{\ell=0}^{2N-1} \dot{x}_\ell(t) \partial_x M_\ell(x), \tag{B.3}$$

where $v(x, t)$ is governed by

$$-\frac{1}{\lambda} \partial_x^{-2} \partial_t v = \partial_x^2 v - W'(v) + h(t). \tag{B.4}$$

The function $h(t)$ arises from the integration in x. The other terms arising from the integration vanish owing to the periodicity in x.

In order to estimate the motion of the jth kink, we use M_j' as a test function by multiplying (B.4) and integrating over the domain. Then we obtain

$$\underbrace{\int_0^L \frac{1}{\lambda} \sum_{\ell=0}^{2N-1} \dot{x}_\ell \partial_x M_j \partial_x^{-1} M_\ell \, \mathrm{d}x}_{A} = \underbrace{\int_0^L (\partial_x^2 v - W'(v)) \partial_x M_j \, \mathrm{d}x}_{B} + \underbrace{\int_0^L h \partial_x M_j \, \mathrm{d}x}_{C}. \tag{B.5}$$

Contribution A can be written as

$$A = -\frac{1}{\lambda} \sum_{\ell=0}^{2N-1} \dot{x}_\ell \int_0^L \int_0^L \partial_x M_j(x) \mathcal{G}_2(x - x') \partial_x M_\ell(x') \, \mathrm{d}x \, \mathrm{d}x', \tag{B.6}$$

where $\mathcal{G}_2$ is the Green function solution of

$$-\partial_x^2 \mathcal{G}_2(x) = \delta(x).$$

$\partial_x M_j$ and $\partial_x M_\ell$ are two well separated functions which contribute to the integral in (B.6), respectively, in the close vicinity of x_j and x_ℓ. By expanding $\mathcal{G}_2(x - x')$ near $\mathcal{G}_2(x_j - x_\ell)$ and summing local contributions using $\int (x - x_j)^2 \partial_x M_j \, \mathrm{d}x = (-1)^j \pi^2 \Gamma / 6s^2$ and $\iint |x - x'| \partial_x M_j \partial_x M_\ell \, \mathrm{d}x \, \mathrm{d}x' = 4\Gamma^2/s$, we obtain

$$A = -\frac{4\Gamma^2}{\lambda} \sum_{\ell=0}^{2N-1} \dot{x}_\ell \left((-1)^{j-\ell} \mathcal{G}_2(x_j - x_\ell) + (-1)^{j-\ell} \frac{\pi^2}{12Ls^2} - \frac{1}{2s} \delta_{j-\ell} \right). \tag{B.7}$$

Using the expression for $\mathcal{G}_2$ within the interval $[0, L]$, one obtains

$$A = -\frac{2L\Gamma^2}{\lambda} \sum_{\ell=0}^{2N-1} (-1)^{j-\ell} \dot{x}_\ell \left(\frac{((x_j - x_\ell)[L])^2}{L^2} - \frac{(x_j - x_\ell)[L]}{L} + \frac{1}{6} + \frac{\pi^2}{24L^2 s^2} - \frac{1}{4Ls} (-1)^{j-\ell} \delta_{j-\ell} \right). \tag{B.8}$$

Contribution B is expanded using

$$W'(v) = W'(M_j) + W''(M_j) \tilde{v}_j + W'_{NL}(M_j, \tilde{v}_j). \tag{B.9}$$

Like $\tilde{v}_j$, W'_{NL} is small in the vicinity of the jth kink but finite at large distance. We have

$$B = -\int_O^L W'_{NL} \partial_x M_j \, \mathrm{d}x + \int_O^L (\partial_x^2 M_j - W'(M_j)) \partial_x M_j \, \mathrm{d}x + \int_O^L (\partial_x^2 \tilde{v}_j - W''(M_j) \tilde{v}_j) \partial_x M_j \, \mathrm{d}x. \tag{B.10}$$

The second integral in (B.10) vanishes and the third one vanishes also after integration of its first term by part. Therefore, we are left with

$$B = -\int_O^L W'_{NL} \partial_x M_j \, dx. \tag{B.11}$$

Using (2) we find

$$W'_{NL} = \frac{2s^2}{\Gamma^2} \tilde{v}_j^2 (3M_j + \tilde{v}_j).$$

In the vicinity of x_j, $\tilde{v}_j$ is of the order of the tails of $M_{j+1}(x_j) - M_{j+1}(-\infty)$ and $M_{j-1}(x_j) - M_{j-1}(\infty)$, that is $O(\max(e^{-2s(x_{j+1}-x_j)}, e^{-2s(x_j-x_{j-1})}))$. In the vicinity of x_{j+1} and x_{j-1}, $\tilde{v}_j$ is $O(1)$ while $\partial_x M_j$ is $O(e^{-2s(x_{j+1}-x_j)})$ and $O(e^{-2s(x_j-x_{j-1})})$. Therefore, the two main contributions to B in (B.11) arise from the vicinities of x_{j+1} and x_{j-1}. In the vicinity of x_{j+1} we use

$$\tilde{v}_j = M_{j+1} + \epsilon_{j+1} \Gamma$$

so that

$$\tilde{v}_j^2 (3M_j + \tilde{v}_j) = \epsilon_j \Gamma^3 (2 - \tanh s(x - x_{j+1}))(1 + \tanh s(x - x_{j+1}))^2.$$

Using also

$$\partial_x M_j = 4s\epsilon_j \Gamma \, e^{-2s(x-x_j)}$$

and replacing in (B.11) with similar contributions from the vicinity of x_{j-1}, we obtain

$$B = -32s^2 \Gamma^2 (e^{-2s(x_{j+1}-x_j)} - e^{-2s(x_j-x_{j-1})}). \tag{B.12}$$

Finally, contribution C gives

$$C = 2\epsilon_j \Gamma h(t). \tag{B.13}$$

Summarizing the results, one gets

$$\frac{2L\Gamma^2}{\lambda} \sum_{\ell=0}^{2N-1} (-1)^{j-\ell} \left(\frac{((x_j - x_\ell)[L])^2}{L^2} - \frac{(x_j - x_\ell)[L]}{L} + \frac{1}{6} + \frac{\pi^2}{24L^2s^2} - \frac{1}{4Ls}(-1)^{j-\ell}\delta_{j-\ell} \right) \dot{x}_\ell$$
$$= 32s^2\Gamma^2(e^{-2s(x_{j+1}-x_j)} - e^{-2s(x_j-x_{j-1})}) - 2\epsilon_j \Gamma h(t). \tag{B.14}$$

Eq. (B.14) shows that two neighboring kink and antikink attracts themselves. A stationary solution is obtained when B vanishes for all values of j. This condition is satisfied if the kinks and antikinks are equispaced over the interval $[0, L]$. Then, $h(t) = 0$.

Eq. (B.14) can be used to determine the motion of the kinks far from the equilibrium, under the condition that the kinks and antikinks remain far enough to satisfy the approximations of the above calculation.

The calculation of Kawasaki and Ohta [12] slightly differs from our own and is limited to the leading order. They fail to take into account the exponential variation of $\tilde{v}_j$ near x_{j+1} and x_{j-1}. Therefore, their result for the leading order of B contains an error, being too small by a factor of 2.

Appendix C. Green function in the periodic domain and calculations of coupling coefficient

Within the periodic domain $[0, L]$, the δ function is made periodic by adding a constant value $-1/L$ everywhere but at the origin. One can also use

$$\delta(x) = \frac{1}{L} \sum_{n \neq 0} \exp\left(i\frac{2\pi n}{L} x\right).$$

The solution to

$$\partial_x^n \mathcal{G}_n(x) = -\delta(x)$$

is

$$\mathcal{G}_n(x) = L^{n-1} g_n\left(\frac{x}{L}\right),$$

where

$$g_1(x) = [1] - \tfrac{1}{2}, \qquad g_2(x) = \tfrac{1}{2}((x[1])^2 - x[1] + \tfrac{1}{6}), \quad g_3(x) = \tfrac{1}{4}(\tfrac{2}{3}(x[1])^3 - (x[1])^2 + \tfrac{1}{3}x[1]),$$

$$g_4(x) = \tfrac{1}{24}((x[1])^4 - 2(x[1])^3 + (x[1])^2 - \tfrac{1}{30}), \quad g_5(x) = \tfrac{1}{720}(6(x[1])^5 - 15(x[1])^4 + 10(x[1])^3 - x[1]),$$

$$g_6(x) = \tfrac{1}{720}((x[1])^6 - 3(x[1])^5 + \tfrac{5}{2}(x[1])^4 - \tfrac{1}{2}(x[1])^2 + \tfrac{1}{42}).$$

where $x[1]$ means x modulo 1.

The calculation of the perturbed motion requires to calculate the Fourier transform

$$\hat{\mathcal{G}}_n(m) \equiv \sum_{j=0}^{2N-1} (-1)^j \mathcal{G}_n\left(\frac{j\Lambda}{2}\right) e^{-i\pi(jm/N)},$$

which can be written as a function of

$$s_m(p) \equiv \sum_{j=0}^{2N-1} (-1)^j \left(\frac{j}{2N}\right)^p e^{-i\pi(jm/N)}.$$

For $m \neq N$, $s_m(p)$ can be calculated using the following relations:

$$P(z, x, J, p) \equiv \sum_{j=0}^{J-1} j^p z^{jx} = \left(\frac{1}{\ln z}\right)^p \partial_x^p \sum_{j=0}^{J-1} z^{jx}, \qquad s_m(p) = \left(\frac{1}{2N}\right)^p P(-e^{-i(\pi m/N)}, 1, 2N, p).$$

We get

$$s_m(0) = 0, \qquad s_m(1) = -\frac{1}{1+a}, \qquad s_m(2) = -\frac{1}{1+a} + \frac{a}{N(1+a)^2},$$

$$s_m(3) = -\frac{1}{1+a} + \frac{3a}{2N(1+a)^2} + \frac{3a(1-a)}{4N^2(1+a)^3},$$

$$s_m(4) = -\frac{1}{1+a} + \frac{2a}{N(1+a)^2} + \frac{3a(1-a)}{2N^2(1+a)^3} + \frac{a(1-4a+a^2)}{2N^3(1+a)^4},$$

$$s_m(5) = \cdots + \frac{5a(1-11a+11a^2-a^3)}{16N^4(1+a)^5}, \qquad s_m(6) = \cdots + \frac{3a(1-26a+66a^2-26a^3+a^4)}{16N^5(1+a)^6},$$

where $a = \exp(-\mathrm{i}\theta_m)$ with $\theta_m = \pi m/N$. We also have

$$s_N(0) = 2N, \qquad s_N(1) = N - \frac{1}{2}, \qquad s_N(2) = \frac{1}{12N}(2N-1)(4N-1), \qquad s_N(3) = \frac{1}{8N}(2N-1)^2,$$

$$s_N(4) = \frac{1}{240N^3}(2N-1)(4N-1)(12N^2 - 6N - 1), \qquad s_N(5) = \frac{1}{96N^3}(2N-1)^2(8N^2 - 4N - 1),$$

$$s_N(6) = \frac{1}{1344N^5}(2N-1)(4N-1)(48N^4 - 48N^3 + 6N + 1).$$

Using these relations, the Fourier transforms are readily calculated. For $m \neq N$, we have

$$\hat{\mathcal{G}}_1(m) = s_m(1) - \tfrac{1}{2}s_m(0) + \tfrac{1}{2} = -\tfrac{1}{2}\mathrm{i}t, \tag{C.1}$$

$$\hat{\mathcal{G}}_2(m) = \tfrac{1}{2}L(s_m(2) - s_m(1) + \tfrac{1}{6}s_m(0)) = \tfrac{1}{8}\Lambda(1 + t^2), \tag{C.2}$$

$$\hat{\mathcal{G}}_3(m) = \tfrac{1}{4}L^2(\tfrac{2}{3}s_m(3) - s_m(2) + \tfrac{1}{3}s_m(1)) = \mathrm{i}\tfrac{1}{32}\Lambda^2 t(1 + t^2) \tag{C.3}$$

with $t = \tan \pi m/2N$. Since the Fourier transform $\hat{\mathcal{G}}_n$ scales as Λ^{n-1}, it depends only on the $\mathrm{O}(1/N^{n-1})$ term in $s_m(n)$. Therefore, the higher order transforms are, for $m < N$:

$$\hat{\mathcal{G}}_4(m) = -\tfrac{1}{384}\Lambda^3(1 + t^2)(1 + 3t^2), \tag{C.4}$$

$$\hat{\mathcal{G}}_5(m) = -\mathrm{i}\frac{\Lambda^4}{1536}t(1 + t^2)(2 + 3t^2), \tag{C.5}$$

$$\hat{\mathcal{G}}_6(m) = \frac{\Lambda^5}{30,720}(1 + t^2)(2 + 15t^2 + 15t^4). \tag{C.6}$$

Using this formalism, it is possible to calculate $\langle v_a, \partial_x^{-n} v_a \rangle$ for even n as

$$\langle v_a, \partial_x^{-n} v_a \rangle = -\frac{1}{L} \int_0^L \int_0^L v_a(x)\mathcal{G}_n(x - x')v_a(x') \, \mathrm{d}x \, \mathrm{d}x'$$

$$= -\frac{1}{L} \sum_{j=0}^{2N-1} \sum_{l=0}^{2N-1} \cos j\theta_m \cos l\theta_m \int_0^L \int_0^L \partial_x M_j(x)\partial_x M_l(x')\mathcal{G}_n(x - x') \, \mathrm{d}x \, \mathrm{d}x'. \tag{C.7}$$

This integral contains two types of contributions. Type I arises from the interaction of distant kinks and type II is a local correction arising from the autocoupling of a given kink and taking into account the discontinuity of $\mathcal{G}_n(x)$ or its derivatives in $x = 0$. At first, we consider only the type I contribution for which $\mathcal{G}_n(x - x')$ can be developed as a Taylor series around $x_j - x_l$ in order to separate the double integration in two independent integrations around the kinks

$$\mathcal{G}_n(x - x') = \mathcal{G}_n(\tfrac{1}{2}(j - l)\Lambda) + \mathcal{G}_{n-1}(\tfrac{1}{2}(j - l)\Lambda)((x - x_j) - (x' - x_l))$$

$$+ \tfrac{1}{2}\mathcal{G}_{n-2}(\tfrac{1}{2}(j - l)\Lambda)((x - x_j) - (x' - x_l))^2 + \cdots.$$

Now we replace in (C.7) and calculate the local contributions using

$$\int \partial_x M_j \, \mathrm{d}x = 2\Gamma(-1)^j, \qquad \int (x - x_j)\partial_x M_j \, \mathrm{d}x = 0, \qquad \int (x - x_j)^2\partial_x M_j \, \mathrm{d}x = \frac{\pi^2\Gamma}{6s^2}(-1)^j.$$

We also expand the trigonometric factor and find that the only nonvanishing contribution depends on $j - l$. After relabeling, we obtain

$$\langle v_a, \partial_x^{-n} v_a \rangle_I = -\frac{4\Gamma^2}{\Lambda} \sum_{j=0}^{2N-1} \cos \frac{\pi m j}{N} (-1)^j \mathcal{G}_n \left(\frac{j\Lambda}{2} \right) - \frac{\pi^2 \Gamma^2}{3s^2 \Lambda} \sum_{j=0}^{2N-1} \cos \frac{\pi m j}{N} (-1)^j \mathcal{G}_{n-2} \left(\frac{j\Lambda}{2} \right),$$

i.e.:

$$\langle v_a, \partial_x^{-n} v_a \rangle_I = -\frac{4\Gamma^2}{\Lambda} \hat{\mathcal{G}}_n(m) - \frac{\pi^2 \Gamma^2}{3s^2 \Lambda} \hat{\mathcal{G}}_{n-2}(m) + \mathrm{O}(\Lambda^{n-6}) \tag{C.8}$$

for even n. A similar relation is obtained for odd n:

$$\langle v_a, \partial_x^{-n} v_b \rangle_I = -\frac{4\Gamma^2}{\Lambda} \frac{1}{i} \hat{\mathcal{G}}_n(m) - \frac{\pi^2 \Gamma^2}{3s^2 \Lambda} \frac{1}{i} \hat{\mathcal{G}}_{n-2}(m) + \mathrm{O}(\Lambda^{n-6}). \tag{C.9}$$

The local type-II contributions must be examined case by case. For $n = 2$, $\mathcal{G}_2(x)$ is continuous in $x = 0$ but its derivative is not. Near $x = 0$, we have

$$\mathcal{G}_2(x) = \frac{L}{2} \left(\frac{1}{6} - \left| \frac{x}{L} \right| + \frac{x^2}{L^2} \right).$$

The two terms $(1/6) + (x^2/L^2)$ are taken into account in type-I contribution. The complementary contribution is

$$\langle v_a, \partial_x^{-2} v_a \rangle_{II} = \frac{1}{2\Lambda} \iint \partial_x M(x) \partial_x M(x') |x - x'| \, \mathrm{d}x \, \mathrm{d}x'.$$

After a bit of algebra, we obtain

$$\langle v_a, \partial_x^{-2} v_a \rangle_{II} = \frac{2\Gamma^2}{\Lambda s}$$

and finally

$$\langle v_a, \partial_x^{-2} v_a \rangle = -\frac{\Gamma^2}{2} (1 + t^2) + \frac{2\Gamma^2}{\Lambda s}. \tag{C.10}$$

For $n = 4$, $\mathcal{G}_4(x)$ has a discontinuity on its third derivative in $x = 0$. It brings an $\mathrm{O}(1/\Lambda)$ correction in $\langle v_a, \partial_x^{-4} v_a \rangle$, which is of higher order than the terms in (C.9).

For odd orders, including $n = 1$, the sine factor cancels the type-II contribution. Notice that for $n = 1$, $\mathcal{G}_1(x)$ is discontinuous in $x = 0$. We have arbitrarily assumed that $\mathcal{G}_1(0) = 0$ in (C.7) but this is not important since only the imaginary part of $\hat{\mathcal{G}}_1(m)$ is used in the sine transform.

Some other quantities may need to be calculated, of the type $\langle f v_a, \partial_x^{-n} v_a \rangle$ where n is odd and f is a period-Λ nonlocalized function which is odd over the kinks. In this case, the nonvanishing contributions are those arising from the odd derivatives of $\mathcal{G}_n$. At leading order, we obtain

$$\langle f v_a, \partial_x^{-n} v_a \rangle = -\frac{2\Gamma}{\Lambda} \hat{\mathcal{G}}_{n-1}(m) \int x f(x) \partial_x M(x) \, \mathrm{d}x + \cdots. \tag{C.11}$$

The same expression holds when v_a is replaced by v_b. The case $n = 1$ is special, we have

$$\langle f v_a, \partial_x^{-1} v_a \rangle = \frac{1}{2\Lambda} \int f(x) \partial_x M^2(x) \, \mathrm{d}x.$$

Appendix D. The effect of mean advection

The case $\gamma \neq 0$ has been studied numerically and near the linear limit r_0 (see Section 4.1) in Ref. [5]. It is possible to study the stability properties of steady solutions for small r in the same way as for $\gamma = 0$ but this is to the price of a considerable increase of complexity in the algebra. It is beyond the scope of this manuscript to describe the details of these cumbersome calculations. We provide here the results without demonstration.

When $\gamma \neq 0$, the equilibrium positions of the kinks and antikinks are given by

$$x_{2p} = p\Lambda - \tfrac{1}{4}\Delta, \qquad x_{2p+1} = (2p+1)\tfrac{1}{2}\Lambda + \tfrac{1}{4}\Delta,$$

where Δ is related to γ by

$$16\Gamma \, \mathrm{e}^{-s\Delta} \sinh s\Delta = -\frac{\Delta\Gamma}{\Lambda} + \gamma. \tag{D.1}$$

We define also $d = \Delta/\Lambda$.

Similarly to Section 4.1, it is convenient to expand the displacements of the kinks with respect to the equilibrium in terms of Fourier components. One has now to separate the kinks and antikinks as

$$\delta x_{2p} = \sum_{m=0}^{N-1} \psi_m^- \mathrm{e}^{\mathrm{i}\pi(2mp/N)}, \qquad \delta x_{2p+1} = \sum_{m=0}^{N-1} \psi_m^+ \mathrm{e}^{\mathrm{i}\pi((2p+1)m/N)}.$$

By combining these components into

$$\Phi_m = \frac{1}{\sqrt{2}} \begin{pmatrix} 1 & 1 \\ \mathrm{e}^{-\mathrm{i}\theta_m} & \mathrm{e}^{\mathrm{i}\theta_m} \end{pmatrix} \begin{pmatrix} \psi_m^- \\ \psi_m^+ \end{pmatrix},$$

we obtain

$$\dot{\Phi}_m = \frac{\mathcal{A}\sin^2\theta_m}{\mathcal{E}_m} \begin{pmatrix} 1 - \mathcal{C}\cosh s\Delta - \mathcal{Q}_m & 0 \\ 0 & 1 - \mathcal{C}\cosh s\Delta + \mathcal{Q}_m \end{pmatrix} \Phi_m \tag{D.2}$$

with

$$\mathcal{A} = \frac{128\lambda \, \mathrm{e}^{-s\Lambda}}{(1-d^2)\Lambda} D, \qquad \mathcal{E}_m = 1 - \frac{4}{s\Lambda(1-d^2)} + \frac{4\sin^2\theta_m}{s^2\Lambda^2(1-d^2)}, \qquad \mathcal{B} = \frac{d\cosh s\Delta - \sinh s\Delta}{D},$$

$$\mathcal{C} = \frac{2}{s\Lambda D}, \qquad D = \cosh s\Delta - d\sinh s\Delta, \qquad \mathcal{Q}_m = (\mathcal{B} + 2\mathcal{C}\sinh s\Delta + \tfrac{1}{2}\mathcal{C}^2(\cosh 2s\Delta + \cos 2\theta_m))^{1/2}.$$

This result generalizes (18).

Now, the stabilization effect by friction is still given at first order of the perturbative expansion for small r. We first need to define

$$\rho_m = 2(\mathcal{B}\cos^2\theta_m + \mathcal{Q}_m \sin^2\theta_m)^{1/2}$$

$$\cos\phi_{1m} = \frac{2}{\rho_m}(\mathcal{B}\cos\theta_m), \qquad \sin\phi_{1m} = \frac{2}{\rho_m}(\mathcal{Q}_m \sin\theta_m), \qquad \cos\phi_{2m} = \frac{2}{\rho_m}(\mathcal{B} + \mathcal{C}\sinh s\Delta \sin^2\theta_m),$$

$$\sin\phi_{2m} = -\frac{1}{\rho_m}(\mathcal{C}\sin 2\theta_m \cosh s\Delta).$$

The stabilization effect is

$$\sigma_1 = -r + \frac{r \sin^2\theta_m}{2} \left(1 - d^2 - \frac{4}{s\Lambda} \right)$$

$$\times \left(1 + d \sin\theta_m \sin(\phi_{2m} - \phi_{1m}) - \cos\theta_m \cos(\phi_{2m} - \phi_{1m}) - \frac{2\sin^2\theta_m}{s\Lambda} \right)^{-1}. \tag{D.3}$$

These results have been checked numerically with the same accuracy as those presented for $\gamma = 0$.

In the case of large Λ and when d is not small, that is when the asymmetry is strong, we can neglect all terms $O(e^{-s\Delta})$ in front of terms which are $O(1)$ or larger. Eqs. (D.2) and (D.3) then simplify considerably. We obtain

$$\dot{\Phi}_m = \frac{128 s^3 \lambda \, e^{-s(\Lambda-\Delta)}}{(1+d)\mathcal{E}_m \Lambda} \begin{pmatrix} ((1-d)s\Lambda)^{-1} & 0 \\ 0 & 1 \end{pmatrix} \Phi_m \tag{D.4}$$

and

$$\sigma_1 = -r + \frac{r}{2} \left((1-d^2) - \frac{4}{s\Lambda} \right) \left(1 + d - \frac{2}{s\Lambda} \right)^{-1}. \tag{D.5}$$

As a consequence, the critical value for friction is, at leading order:

$$r_c = \frac{256 s^3 \lambda \, e^{-s(\Lambda-\Delta)}}{(1+d)^2 \Lambda}. \tag{D.6}$$

Notice that this relation is not valid for small d and does not match (39) for $d = \Delta = 0$.

References

[1] P. Rhines, Waves and turbulence on a beta-plane, J. Fluid Mech. 69 (1975) 417–443.
[2] G. Williamson, Planetary circulation. I. Barotropic representation of Jovian and terrestrial turbulence, J. Atmos. Sci. 35 (1978) 1399–1426.
[3] P. Rhines, Jets, Chaos 4 (1994) 313–339.
[4] G. Vallis, M. Maltrud, Generation of mean flow and jets on a beta-plane and over topography, J. Phys. Oceanogr. 23 (1993) 1346–1362.
[5] A. Manfroi, W. Young, Slow evolution of zonal jets on the beta-plane, J. Atmos. Sci. 56 (1999) 784–800.
[6] U. Frisch, B. Legras, B. Villone, Large-scale Kolmogorov flow on the beta-plane and resonant wave interactions, Physica D 94 (1996) 36–56.
[7] L. Meshalkin, Y. Sinai, Investigation of the stability of a stationary solution of a system of equations for the plane movement of an incompressible viscous liquid, Appl. Math. Mech. 25 (1961) 1700–1705.
[8] G. Sivashinsky, Weak turbulence in periodic flows, Physica D 17 (1985) 243–255.
[9] A.A. Nepomnyashchyi, On the stability of the secondary flow of a viscous fluid in an infinite domain, Appl. Math. Mech. 40 (1976) 886–891.
[10] Z. She, Metastability and vortex pairing in the Kolmogorov flow, Phys. Lett. A 124 (1987) 161–164.
[11] B. Legras, U. Frisch, B. Villone, Dispersive stabilization of the inverse cascade for the Kolmogorov flow, Phys. Rev. Lett. 82 (22) (1999) 4440–4443.
[12] K. Kawasaki, T. Ohta, Kink dynamics in one-dimensional nonlinear systems, Physica A 116 (1982) 573.
[13] J. Pedlosky, Geophysical Fluid Dynamics, 2nd ed., Springer, New York, 1987.
[14] A. Manfroi, W. Young, Stability of β-plane Kolmogorov flow, Physica D 162 (3-4) (2002) 208–232.
[15] B. Legras, On the stability of β-plane Kolmogorov flow, in preparation.
[16] Y. Lee, L. Smith, Stability of Rossby waves in th β-plane approximation, Physica D, 2002, submitted for publication.
[17] P. Bates, J. Xun, Metastable patterns for the Cahn–Hilliard equation, Part II, J. Diff. Eq. 117 (1995) 165–216.
[18] U. Frisch, B. Legras, B. Villone, Large-scale dynamics of the Kolmogorov flow on the beta-plane, in: R. Benzi (Ed.), Advances in Turbulence, Proceedings of the Fifth European Turbulence Conference, Kluwer Academic Publishers, Dordrecht, 1995, pp. 138–140.
[19] R.H. Kraichnan, Inertial ranges in two-dimensional turbulence, Phys. Fluids 10 (1967) 1417–1423.
[20] B. Legras, P. Santangelo, R. Benzi, High-resolution numerical experiments for forced two-dimensional turbulence, Europhys. Lett. 5 (1) (1988) 37–42.